1990

Surface geometry evaluation through digital image analysis enhanced shaow moiré

Jen E. Andrew Liao
Lehigh University

Surface Geometry Evaluation Through Digital Image Analysis
Enhanced Shadow Moire

By

Jen E Andrew Liao

A Thesis

Presented to The Graduate Commitee

of Lehigh University

in candidacy for the Degree of

Master of Science

in

Department of Mechanical Engineering and Mechanics

January 1990

CONTENTS

Certificate of Approval

The undersigned hereunder accepts and approves this thesis in partial fulfillment of the requirements for the degree of master of science in Mechanical Engineering and Mechanics.

Professor in charge
Dr. Arkady S. Voloshin

Department Chairman
Dr. Fazil Erdogan

Acknowledgements

I would like to thank Dick Town and all the machine shop crew members for their support and assistance in times of difficulty.

I would also like to acknowledge the support of the Benjamin Franklin Institute which provided the funds for this project.

Finally, I would like to express my deepest appreciation to Dr. Arkady S. Voloshin for his continued support throughout this thesis. His expertise in the field contributed the greater part of this thesis.

This thesis is dedicated to my parents for their constant support and encouragement.

Abstract

This thesis describes a simple and accurate system to control product's geometry based on combination of Shadow Moire and Digital Image Analysis. The developed system is able to measure out-of-plane displacement on the specimen with 0.01 mm sensitivity. The developed Shadow Moire and Digital Image Analysis integrated system can be applied in industrial environment for non-destructive evaluation and quality control of the part's geometry.

List of Figures

Specimen 1 (Density 20 lines/inch)

Specimen 1 (Density 50 lines/inch)

Specimen 2 (Density 20 lines/inch)

Specimen 2 (Density 50 lines/inch)

List of Symbols

I_o = Average background light intensity

I_i = Light intensity amplitude of the first harmonic

$I(x)$ = Light intensity at a point of coordinate x in the image plane

N = Fringe Number

P = Grating pitch

U = Displacement in the direction of the x axis

X = Coordinate

Z = Distance (Out-Of-Plane Displacement)

ρ = Relative displacement of the two grids

β = Angle between the camera and normal to the moire screen

θ = Angle between the light source and normal to the moire screen

1. Introduction

Development of a non-contact evaluation technique to control the product's geometry is of critical importance. In some cases, the product has an inward or outward dimple within 0.01 mm range or the product's surface has unwanted curvature variation which can be extremely difficult to detect by human eye. The flexibility of the well known Shadow Moire method [1] associated with Digital Image analysis [2] can provide an accurate measurement of the specimens geometry. The method of shadow moire was applied to investigate the human body topography [3]. Moire interferometry was extended to the out-of-plane displacement measurements as well [4].

Shadow moire pattern appears when a test surface is placed close to the ruling and illuminated by a collimated light beam at an angle θ. The light beam will project the ruling on the testing surface and the interferences between the ruling and its shadow will occur. This type of optic phenomenon applied to study of the out-of-plane displacement was thoroughly investigated by Theocaris [5].

The resulting moire pattern is the contour map of the surface geometry. The sensitivity of this technique is determined by the pitch of the "master" ruling. Use of 20 lines/mm [6] for very small depth variations and 0.3 lines/mm for investigation of big panel buckling [7] was reported. However, use of 20 lines/mm pitch requires extreme closeness to the specimen and can be used for small areas only. To overcome this problem, especially in the situation where the sensitivity of one grating alone is not sufficient to map the whole surface, a technique was developed [8], which utilized two superimposed gratings with different pitches.

The digital image analysis enhanced shadow moire technique described here is based on the combination of two well known and developed methods - shadow moire and modern digital image analysis. This combination allows significant increase of the sensitivity of shadow moire technique by utilizing the ability of digital image analysis system to acquire whole field light intensity information and process this information to predict the related displacement field.

2.Analysis of In-plane Moire Fringes Formation.

2.1 Fundamental Property of In-Plane Moire Fringes (Nonrotational Case)

In this section the formation of in-plane fringes under a nonrotation condition will be explained. The relative displacement of one grating with respect to another of a different pitch will also be illustrated. The purposes of this chapter is to give insight into out-of-plane moire fringes formation which are described in subsequent chapters.

Consider now the interference of two gratings with lines parallel to each other, but of different pitches p and p_1. The interference can be visualized as being obtained from uniform contraction or elongation of one grating with respect to the other. This mechanism of fringe formation is shown in Figure 2.1. A dark fringe will appear at the points where an opaque strip falls over a transparent strip. When two opaque strips coincide, there is a maximum of light intensity and a light fringe appears.

In figure 2.1, a point Q is at the left edge where the grating line of specimen and master grating coincide, while point R undergoes a displacement equal to the pitch P due to the elongation and is now shown by Q′. The center line of the light fringe which goes through Q′ indicates a displacement in the direction of the principal section equal to P.

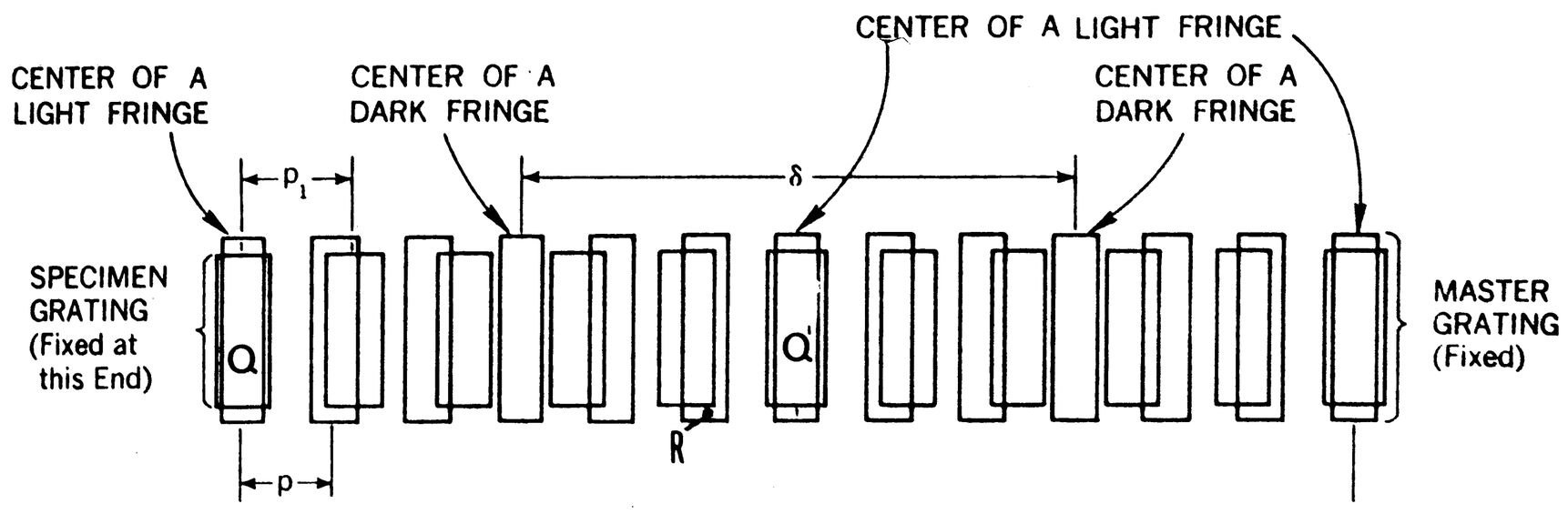

Figure 2.1 Formation of fringe without relative rotation of the gratings

It can be concluded that the moire pattern gives the relative displacement in the direction of principal section and the final position of the point Q' in the deformed state of the model has undergone a displacement P.

The following relationship is also obvious, let M represent the number of lines of the master grating that fall between two fringes,

$$\delta = MP = (M \pm 1)P_1 \quad \ldots\ldots\ldots (2.1)$$

This permits the determination of the specimen pitch :

$$P_1 = P\frac{M}{M \pm 1} = \frac{\delta}{\frac{\delta}{P} \pm 1} \quad \ldots\ldots (2.2)$$

The plus-or-minus sign (±) indicated that the specimen pitch either increases (minus sign) or decreases (plus sign) with respect to the master pitch.

2.2 Fundamental Property of In-Plane Moire Fringes (rotational Case)

In this section the formation of fringes under a rotation condition will be investigated. The relationship of distance between fringes which result from a rotation angle θ will also be illustrated.

If the specimen grating is not subjected to elongations or contractions in the direction perpendicular to the grating, but to rotation only, then the phenomenon is one of pure rotation of two like gratings with respect to each other. Such a case is shown in Figure 2.2.

From the geometry of the intersecting lines shown in Figure 2.2.

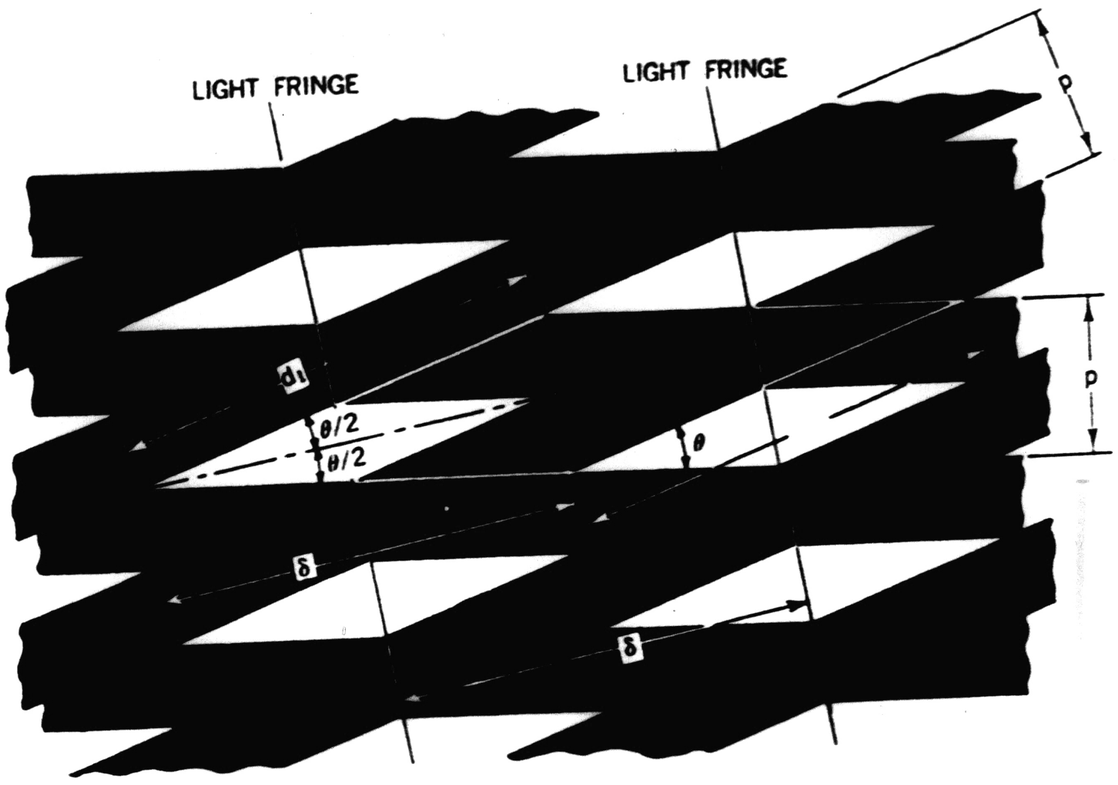

Figure 2.2 - Formation of moire fringes with relative rotation of the gratings.

The length of the side of the rhombus is given by

$$d_1 = \frac{P}{\sin\theta} \quad \ldots\ldots\ldots\ldots (2.3)$$

$$\delta = d_1 \cos\frac{\theta}{2} \quad \ldots\ldots\ldots (2.4)$$

$$\delta = \frac{P \cos\frac{\theta}{2}}{\sin\theta} \quad \ldots\ldots\ldots (2.5)$$

$$\delta = \frac{P}{2\sin\frac{\theta}{2}} \quad \ldots\ldots\ldots (2.6)$$

and, for small angle θ, by

$$\theta = \frac{P}{\delta} \quad \ldots\ldots\ldots\ldots (2.7)$$

Thus, the angle θ can be calculated when the pitch and the distance between fringes are known.

3. Analysis of the shadow moire method

In this chapter the basic principles of shadow moire method to investigate the out-of-plane displacement field will be illustrated.

A master grating[9] is placed close to the surface under examination and this surface is illuminated by a collimated light beam at an angle θ. The opaque lines of the screen will project shadows on the examined surface. The illuminated lines between the shadows will reflect light towards the camera. When the shadows face spaces of the screen, interferences will occur, producing moire' fringes, as shown in Figures 3.1 and 3.2. The shadows depend on the selected illumination angle θ,and on the depth Z (out-of-plane displacement) of the observed point.

A simple count of the obtained fringes gives the displacement

$$U = NP \quad \ldots\ldots\ldots\ldots\ldots\ldots\ldots\ldots (3.1)$$

where

N = Fringe Number
P = Pitch of the master grating

When the grating and the shadow are superimposed, the light can be transmitted only through the space left between the opaque line. In this case a dark fringe occurs when one grating line falls between two lines of the shadow.

Maximum light intensity occurs when on grating has moved a distance of one-half the pitch and falls in front of a line of the shadow. In between these two extremes, the light intensity is proportional to the displacement u. The result of this optical phenomenon will construct a sinusoidal like light intensity curve as illustrated in Figure 3.3.

It can be shown that for a grating with known pitch the relationship between displacement and light intensity is

$$I(x) = I_o + I_1\cos 2\pi\rho(x) + I_2\cos 6\pi\rho(x) \ldots\ldots\ldots (3.2)$$

Where

Io = the average background intensity
I_1, I_2,etc. = the intensity amplitudes of corresponding harmonics (figure 3.3)
$\rho(x)$ = relative displacement of shadow and grating

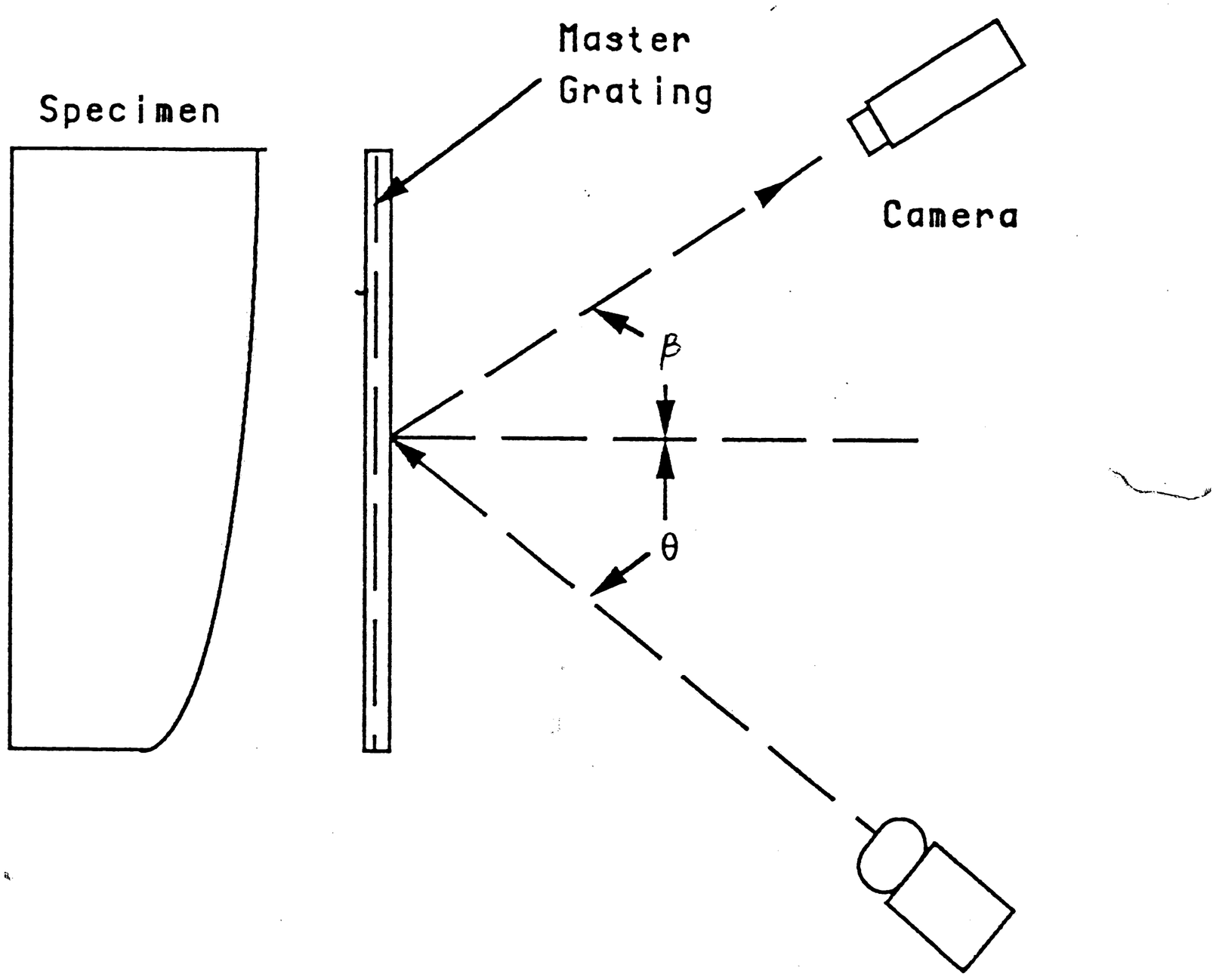

Figure 3.1 Experimental Setup for Shadow Moire

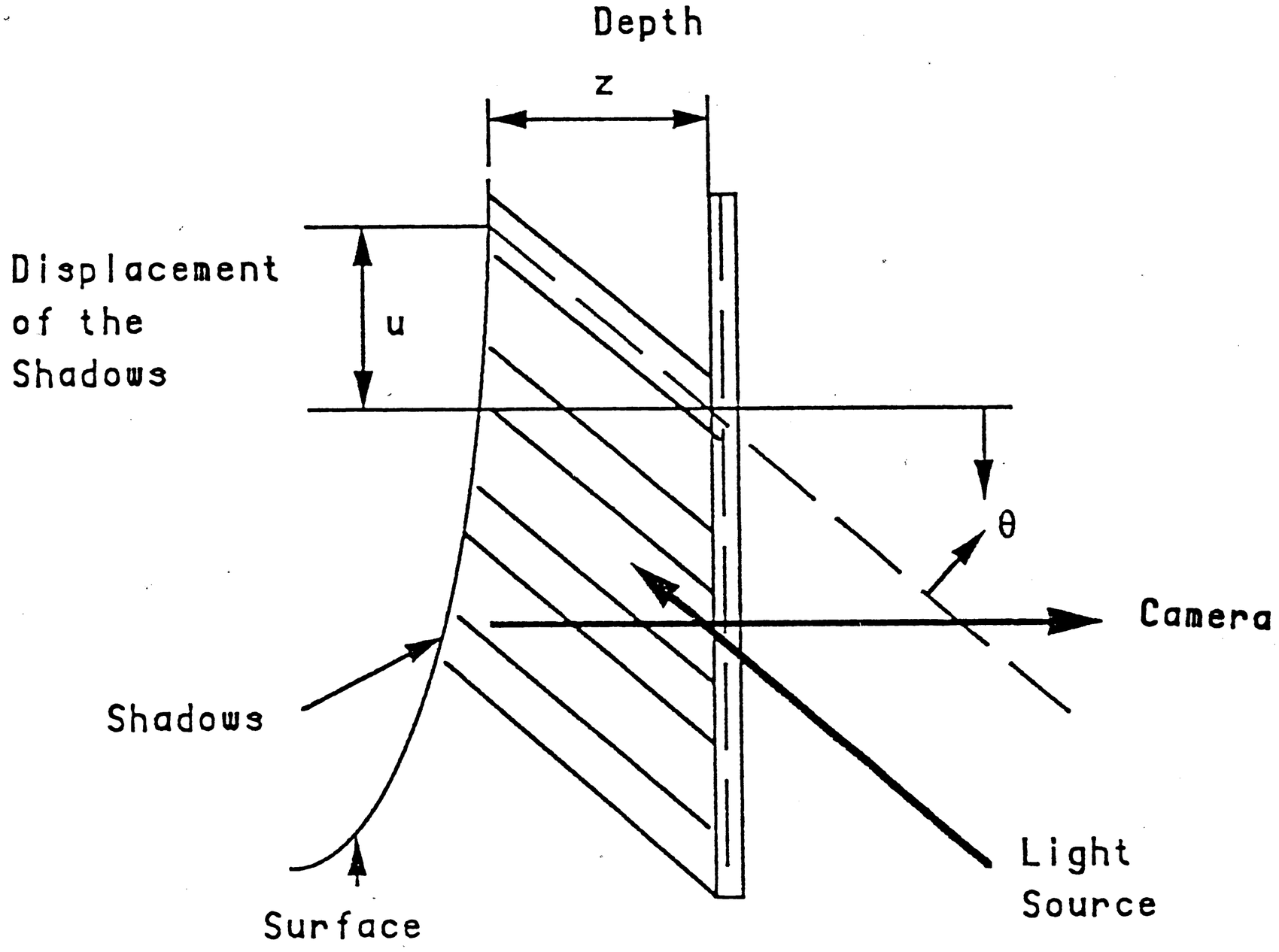

Figure 3.2 Formation of shadow moire fringe

It can be shown that for a grating with known pitch the relationship between displacement and light intensity is

$$I(x) = I_o + I_1\cos 2\pi\rho(x) + I_2\cos 6\pi\rho(x) \ldots\ldots\ldots \quad (3.2)$$

Where

Io = the average background intensity
I_1, I_2, etc. = the intensity amplitudes of corresponding harmonics (figure 3.3)
$\rho(x)$ = relative displacement of shadow and grating

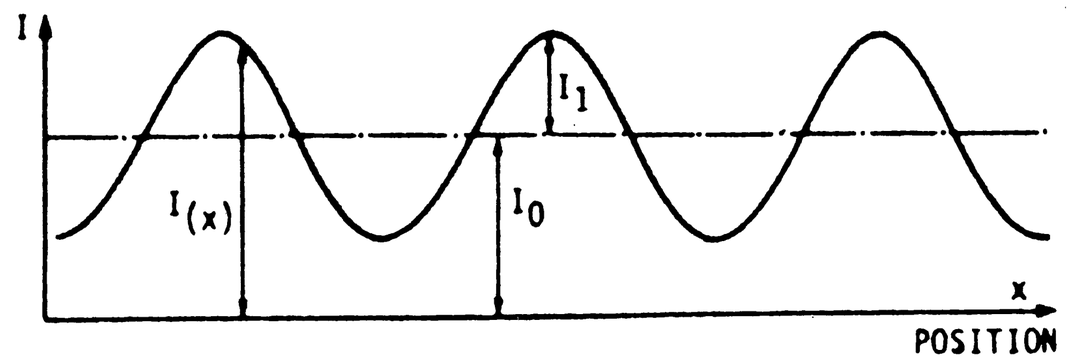

Figure 3.3 Definition of intensity amplitudes

The relative displacement $\rho(x)$ can be expressed through the displacement field u(x). After substitution in eq.(4) one gets

$$I(x) = I_o + I_1 \cos\frac{2\pi u(x)}{P} + I_2 \cos\frac{6\pi u(x)}{P} + \ldots(3.3)$$

Under commonly used condition of filtering the harmonics of order higher than one are usually ignored. Consequently, the light intensity distribution is related to the displacement field as

$$U(x) = \frac{P}{2\pi} \text{ arc cos } (I(x) - I_o)/ I_1 \quad \ldots\ldots\ldots\ldots(3.4)$$

The validity of eq.(3.4) is extended to any displacement fields. But the equation is valid only over one-half fringe of the moir'e pattern, that is, any cycle of change in light intensity from dark to light or light to dark.

In figure 3.3, the distance from grating to the surface Z is given by

$$Z = U/(\tan\theta+\tan\beta) \quad \ldots\ldots\ldots\ldots\ldots\ldots\ldots\ldots\ldots\ldots (3.5)$$

where

β = angle between the normal to the master grating and position of the camera.

θ = angle between the normal to the master grating and position of the collimated light source.

In order to eliminate the distortion in photographic recording, the camera is set perpendicularly to the observed surface, making $\beta = 0$.

The out-of-plane displacement is then given by

$$Z = PN/\tan\theta \quad \ldots\ldots\ldots\ldots\ldots\ldots\ldots\ldots\ldots\ldots (3.6)$$

Combine 3.4 and 3.6 obtain :

$$Z = \frac{P}{2\pi \tan\theta} \arccos (I(x)- I_o)/ I_1 \quad \ldots\ldots (3.7)$$

In this project procedures, that use digital image analysis system to record and process fractional fringe orders, have been developed to investigate the specimen's geometry.

4. Experimental Arrangement

To investigate the suggested procedure for extraction of out-of-plane displacement information from a shadow moire pattern, the following experimental system has to be put together:

A. Light Source :

A bright light source (Figure 4.1), equipped with an adjustable slit parallel to the direction of the master ruling, permitting a large gap between the screen and the observed surface. The standard light source includes a 600 watt quartz halogen, fan-cooled lamp focused on an adjustable slit, with a projection lens, permitting illumination of a (600 x900 mm) area.

B. Master Grating [9] :

Standard Density

0.81.p. mm (20 lines/inch)
21.p. mm (50 lines/inch)
81.p. mm (200 lines/inch)

C. Camera :

The camera[10] used was a Sony black and white video camera model XC-57. This is a solid state camera that has a high resolution CCD (Charge Couple Device) element. The CCD element is composed of an array of 510 by 492 picture elements (pixels).

D : Image Analysis System :

1. PC-AT based image acquisition board[11]

2. High-resolution color monitor for displaying of enhanced image.

3. PC-AT with DOS operating system, B&W monitor keyboard, and software to utilize recorded light intensity for calculation of the out-of-plane displacement field Z.

1. Light Source
2. Master Grating
3. Camera

Figure 4.1 Experimental Set-Up

5. Experimental Procedures

The basic concept of shadow moire method and the apparatus arrangement to investigate the out-of-plane displacement has been introduced in the previous chapter. The aim of this chapter is to describe the experimental procedure in two major steps : A. Experimental set-up, B. Software package to analyze the out-of-plane displacement.

A. Experimental set-up : In order to apply the theory of shadow moire to investigate the out-of-plane displacement, an accurate moire fringe pattern which represents the contour map of the specimen's surface has to be recorded. There are several steps to be followed :

1.The height of camera, master grating, light source, and the examining surface here to be the same.

2.The master grating and the surface under investigation shall be as parallel as possible and in close contact to each other.

3.The camera is set perpendicularly to the master grating surface, and the illumination angle θ[figure 3.1,3.2] between the camera and the light source set at a 45 degree angle. Result of this will provide a multiplication factor $1/\tan\theta=1$ and also eliminate the distortion in photographic recording. Since it is difficult to set correct angle a calibration procedure was developed [chapter 7 (b)].

4.A master grating of a proper density has to be selected based on the dimension and relative depth of the examining surface, to provide a good resolution.

5.The surface to be examined should be reflective. A light spray paint(flat white) will properly diffuse the light.

6.A relatively uniform illumination of the examined surface can be achieved by adjusting the slit on the light source and the distance to the surface.

7.The lens of camera ,light source, and the screen of master grating shall be kept clean.

8.A scale for calculating the actual displacement resulting from the magnification of the camera shall be provided.

B. Software package: The software package can be constructed by any of the languages DT_IRIS[11] supports. In this thesis the Fortran code was selected. The computer software package contains a series of DT_IRIS's library subroutines to acquire and restore the image of the surface, extract the information of light intensity from the investigated area, and plot the data information on the image monitor. Several numerical methods for smoothing data are also included in this package. The steps to calculate the out-of-plane displacement can be presented as follows:

1.Calculate the correct value for $\tan\beta+\tan\theta$(chapter7b)

2.Input the actual length or dimension of the examined region, the pitch of ruling and the appropriate value for $\tan\beta + \tan\theta$ [step 1].

3.Define the boundaries of the line or area under investigation on the display monitor. This can be achieved by using an x-y cursor displayed on the display monitor. This cursor can be activated by mouse. For scanning a line, it is necessary to position the cursor at the beginning and the end of the scan line. For scanning an area, position the cursor at the top left corner and the right bottom corner of the investigated rectangular region. Thus the array of pixel element along the scan region can be constructed and the dimension representing the pixel element on the monitor can also be calculated from the information provided in step 2.

4.The value of light intensity along the scan line can be accomplished by using a DT_IRIS subroutine(ISGETP)[11]. The continuous light intensity curve along the scan line can also be observed on the display monitor by using a DT_IRIS subroutine(ISPUTP)[11].

5.The measured light intensity usually contains random noise caused by the electronic and optical components of the system. Two digital filtering options are provided in this software package: Fourier transform and weight averaging. The choice of option depends on the quality of the image and is decided by the user.

6.The values of I_o and I_1 are not constants through the whole field, this being intrinsic nature of shadow moire techniques (the light source is not normal to the surface). Thus, it is necessary to account for this non-uniformity of light field[chapter 7(A)].

7.Search for maximum and minimum (peaks and valleys)[Figure 6.2] values of the light intensity curve along the scan line after the proper light intensity curve is selected. They will indentify the locations of the half-fringe multiples, and also the location of non-half fringe[Figure 6.2] which is located at the right edge of the light intensity curve [Figure 6.2]. This can be achieved by a specially developed search algorith. The missing and incorrect locations of the peaks and valleys can be adjusted by using the x-y cursor.

8.Assign the fringe value. This is based on the half-fringe multiplication (0.5,1,1.5...) from dark to bright and from bright to dark. The sign of half fringe order depends on the moire pattern and the location of the zero fringe as a reference position (z = 0) to calculate the out-of-plane displacement. The reference position can be obtained by placing the specimen surface in close contact to the ruling screen. The fringe order can be assigned by operator or automatically.

9.Calculate the light intensity amplitudes(I_1) for each half fringe sequence. The amplitude of the non-half fringe(Figure 6.2) at the edge of the light intensity curve is selected from the half fringe before the edge.

10.Apply the equation 3.4 and associate the information of fringe order from step 8 to calculate the out-of-plane displacement. This is done for all half-fringe spans.

11.Calculate the out-of-plane displacement of the non-half fringe section. The variation of the out-of-plane displacement for the non-half fringe section can be referred either to the fringe number before or after the segment.

12.Calculate the average relative error and investigate the absolute fringe value. For the purposes of comparision, the actual shape of the surface under investigation was measured manually, using high-precision(0.05 mm) dial gage mounted on the flat surface. These data was taken at the 12 by 12 locations on each of the two specimens. This specimens were specially prepared for this investigation and they were made to differ one from another by a small value (between 0 and 2 mm).

The average relative error calculation is based on the shadow moire data and the dial gage measurement. The dial gage measurement curve [figure 6.4] is generated by twelve data points from the specimen and curve fit by a second order polynomial. And the shadow moire data is calculated from scanning the image's most central line.

Since the grating is inside the laminated plate and can not touch the specimen one can not decide on the absolute fringe value. In order to compare the shadow moire data and dial gage measurement, the shadow moire data has to be shifted by a constant value.

6.Result

Two specimens[figure 6.1] were selected for this experiment. The blocks differ slightly in the topology of their top curved surfaces. The difference between depths at corresponding coordinates is small; on the order of 2 mm. The results presented in this thesis are based upon the image's most central line, which corresponds to the maximum light intensity of the image.

For specimen 1 the out-of-plane displacements were measured at six scan line as shown in figures 6.5 and 6.6, using two different grating densities of 20 and 50 lines/inch. For each line, fractional half fringe analysis based on equation 3.7 was used to predict out-of-plane displacements. An example of such an analysis for the given scan line of the specimen is shown in figures 6.3 and 6.4.

Figure 6.3 shows observed and corrected light intensity distributions for grating density of 20 line/inch. Curve 1 is the actual measured light intensity distribution, while curve 5 is the corresponding corrected curve.

The need for correction arised from the non-uniformity of the background light intensity as seen in curve 4 and from non-uniformity of the bright fringe peaks and dark fringe peaks as seen in curve 2 and 3 respectively. After correcting the average background light intensity and the peaks light intensities as described later in chapter 7A, the resulting corrected light intensity is given by curve 5. The correction did not significantly change the displacement distribution. only a 0.2 average relative percent difference was found between corrected and original data.

Figure 6.4 shows the out-of-plane displacements as predicted by shadow moire and for comparision by a dial gage. In this figure, curve 2 gives the displacement distribution as observed without correct angle incident correction, while curve 3 is the same distribution but with correction taken into account. Clearly, the correction changed the distribution a lot. 1.2 average relative percent difference is reported between corrected and original data. On the same figure curve 1 shows the displacement distribution as measured by a dial gage. It was noted that the thickness of the glass plate holding the grating (2mm) had to be subtracted from shadow moire predictions of displacements. When doing that, the final displacement distribution becomes as shown in curve 4 which is in excellent agreement with dial gage measurements.

Fig. 6.5 and 6.6 give the distribution map of the out-of-plane displacements along the six scan lines both by shadow moire and by dial gage measurements. Two viewing angles for the specimen are shown. Since the out-of-plane displacements are measured from a reference surface, the displacements are transformed to physical plane representing the shadow moire surface.

The final out-of-plane displacements, by the two methods are given by the displacement contour maps shown in figure 6.7. The maximum displacement average relative error observed for this specimen at the center scaning line is 1.2 percent. Which is acceptable keeping in mind minor inaccuracies produced by method of light intensity correction, noise in the recorded image, precision of the dial gage used and its holder.

For the same specimen 1, but with a grating density of 50 lines/inch., a similar set of graphs were generated, figures 6.8,6.9,6.10,6.11,6.12. In this case the number of fringes produced were higher(12 fringes vs. 5 fringes for the 20 lines/inch case).

Comparable displacements were arrived at using this grating density, from figure 6.9 curve 3 shows the result of taking account of correct angle of light incidence significantly increased accuracy by 1.13 percent and average relative error as related to dial gage measurements stayed within the same order(2.9 percent). The reason this is slightly higher than the case of 20 lines/inch is that aligments of the components could not be identical each time the experiment is repeated. It was noted that the thickness of the glass plate holding the grating (0.8 mm in this case) had to be subtracted from shadow moire predictions of displacements, which is represented by curve 4 in figure 6.14.

For specimen 2 with a grating density of 20 lines/inch similiar observations were recorded as shown in figures 6.13,6.14,6.15,6.16,6.17. Again, figure 6.14 curve 3 shows the result after taking into account the correct angle of light incidence. The accuracy was increased by 1.23 percent in this case. For this specimen comparision of dial gage measurements to shadow moire predictions has shown 1.3 percent difference as seen from figure 6.14 for the distribution of displacement along the center line and from figure 6.17 for the contour map of displacements. The effects of the experimental noise which appears in the margin of the image can also be observed in figures 6.15,6.16 for two different views angle.

For the same specimen 2, but with a grating density of 50 lines/inch., a similar set of graphs were generated, figures 6.18,6.19,6.20,6.21,6.22. Figure 6.18 shows that number of fringes produced were higher(10 fringes vs. 4. fringes for the 20 lines/inch case). When the thickness of the glass plate holding the grating was subtracted from the shadow moire predictions of displacements, the results became closer to the dial gage data (Figure 6.19).

Comparable displacements were measured for 50 lines/inch grating density, when the dial gage was used. Figure 6.19 (curve 3) shows that taking into account correct angle of light incidence significantly increased accuracy by 1.2 percent and average relative error as related to dial gage measurements stayed within the same order(2.76 percent). The reason this is slightly higher that than in the case of 20 lines/inch is that aligments of the components could not be identical each time the experiment is repeated.

It can be concluded that the shadow moire technique is capable of distinguishing topology difference at the order of 0.2 mm for two specimen. This can be seen in figures 6.23,6.24,6.25.

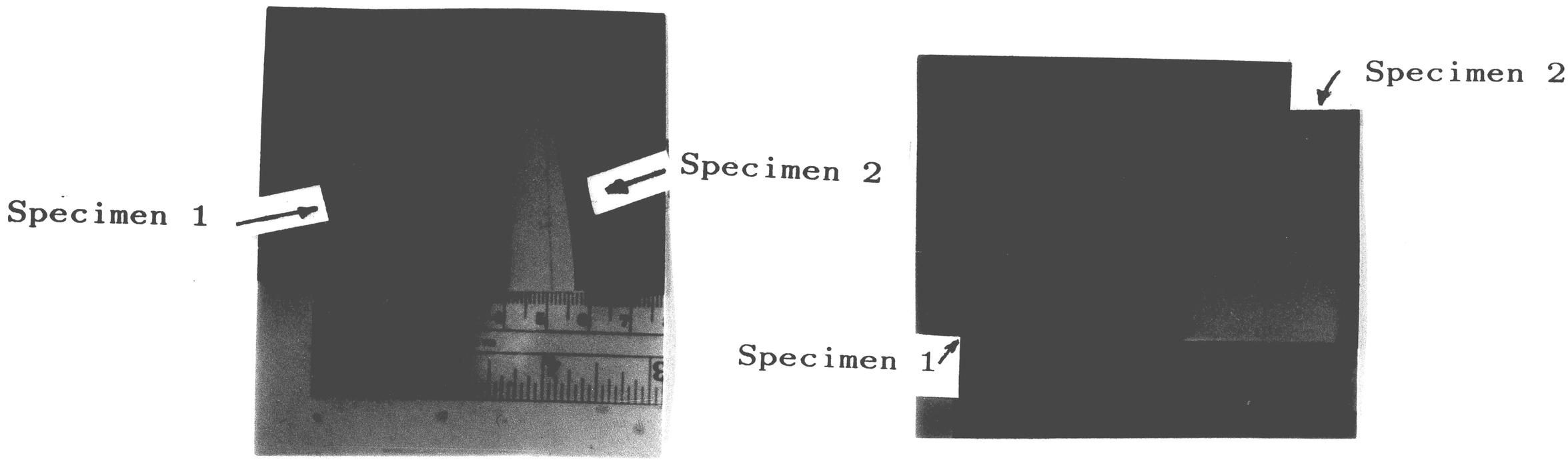

Figure 6.1 Specimen 1 & 2

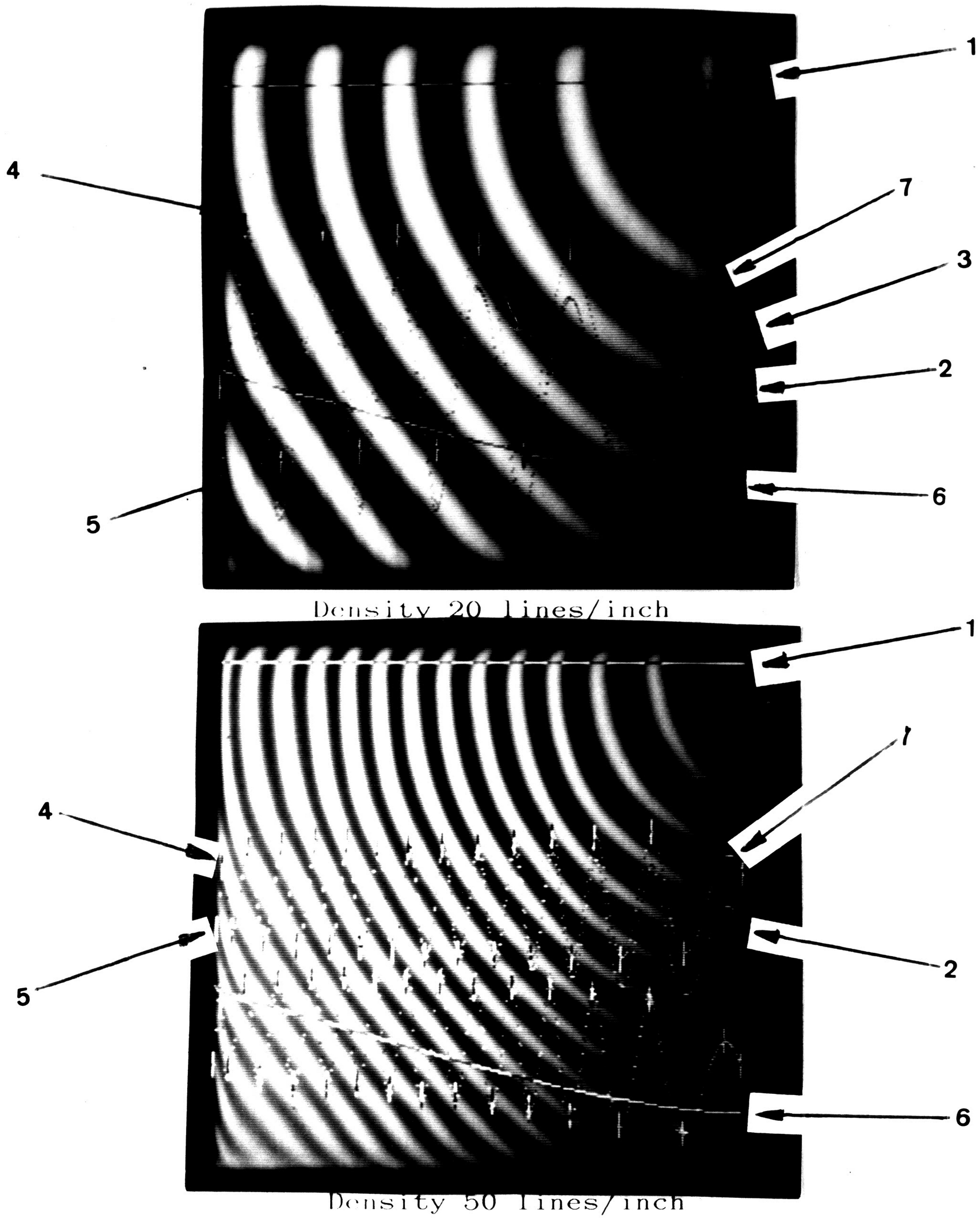

Figure 6.2 Shadow Moire Image

1. Scan line
2. Original light intensity along the scan line
3. Light intensity after taking into account of non-uniform light field
4. Peak of bright fringe
5. Peak of dark fringe
6. Out-of-plane displacement
7. Non-half fringe

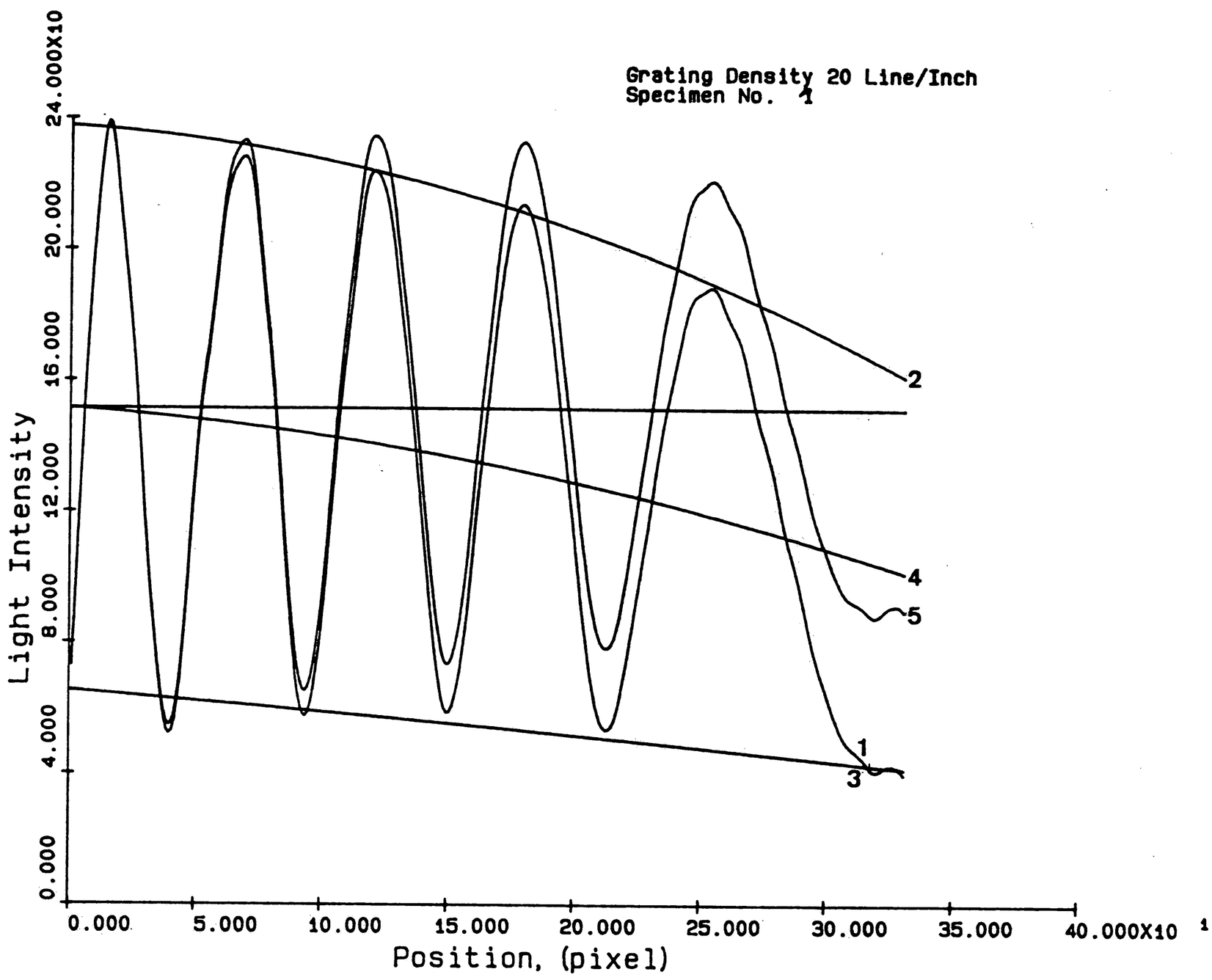

Fig. (**6 3**) Light Intensity Scan And Modification for Non - Uniform Light Intensity

1 - Original light intensity
2 - Curve-fit for bright fringes
3 - Curve-fit for dark fringes
4 - Mean light intensity (between 2 and 3)
5 - Light intensity after shift

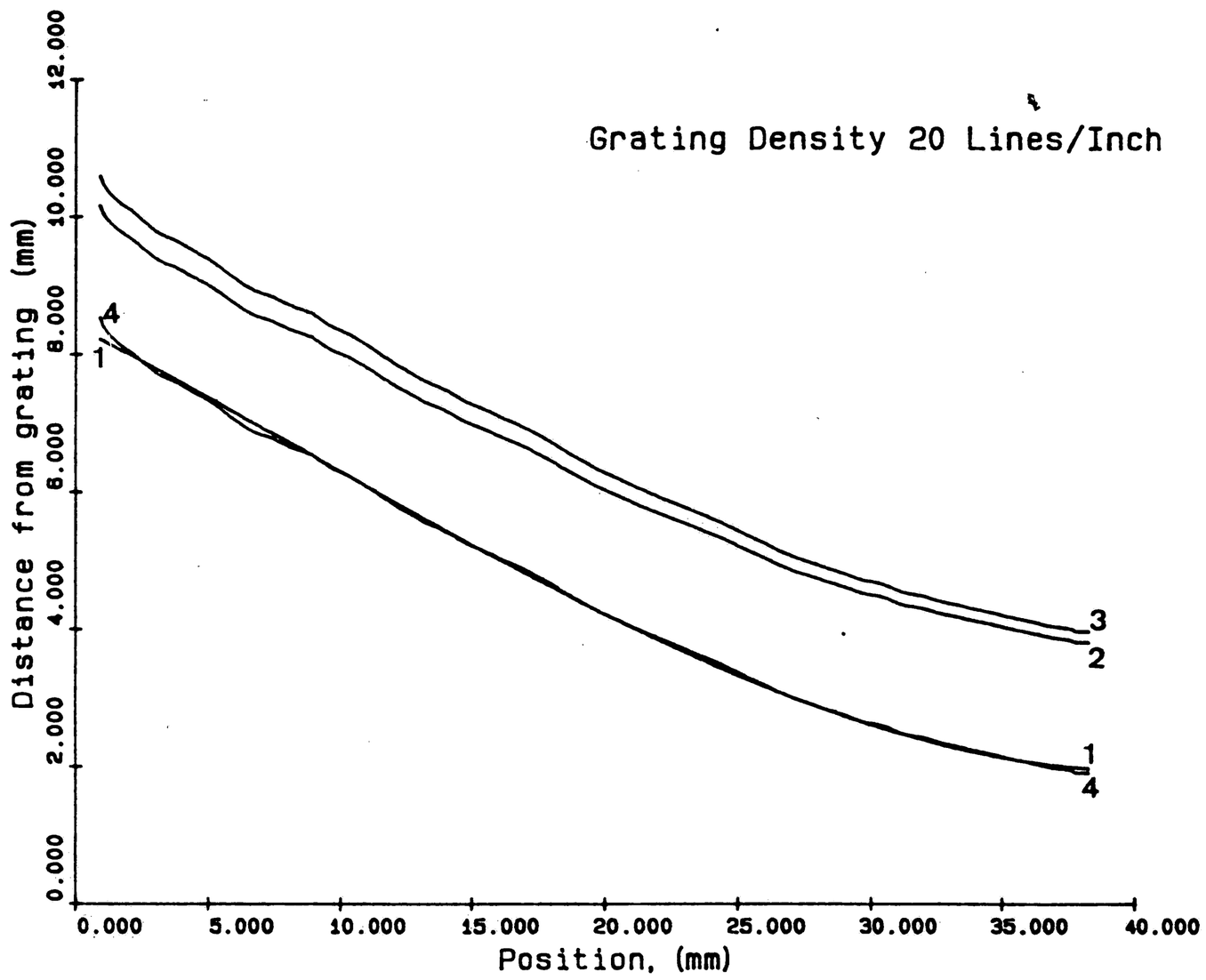

Fig. 6 4 Distance from the grating along the cross-section D-D for specimen 1

1 - Actual depth measured by dial gage

2 - Distance calculated from shadow moire pattern

3 - Distance calculated from shadow moire pattern taking into account correct angle of light incidence

4 - Distance after shift

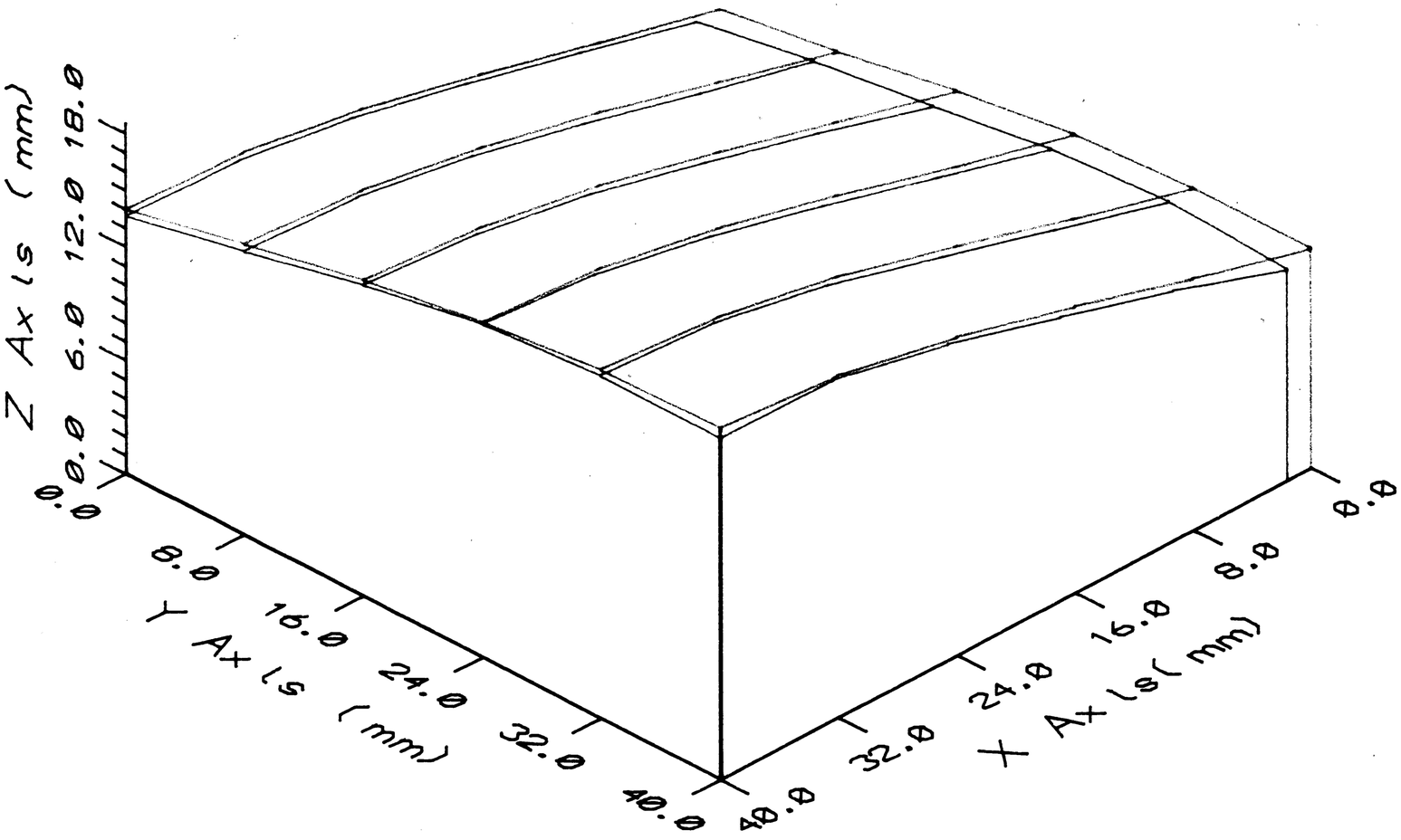

Flg(6 5) Specimen 1, Density 20 l./in.(45 Degree)

—— Shadow Moire
—— Dial Measurement

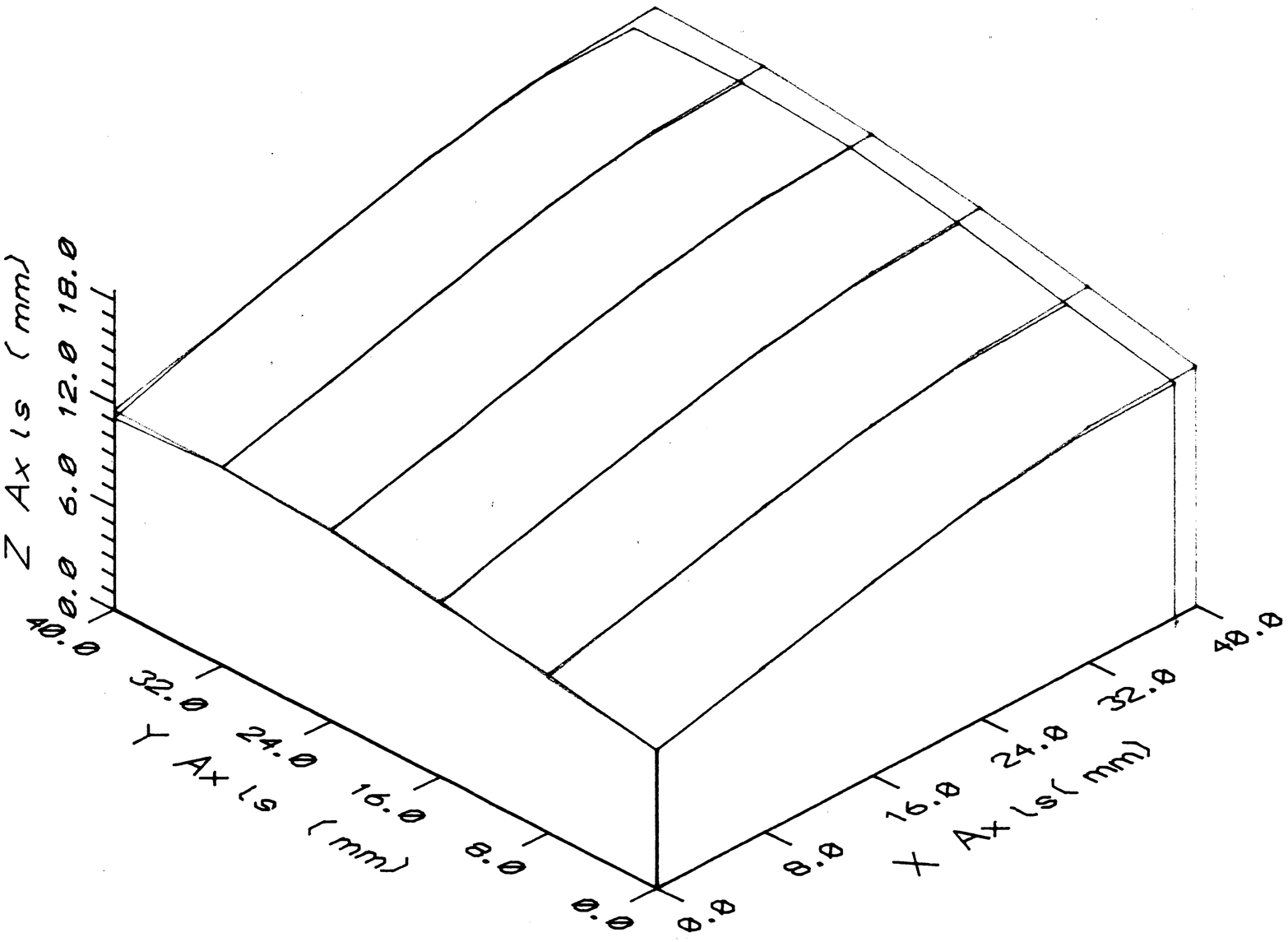

Fig(6.6) Specimen 1, Density 20 l./in.(225 Degree)

—— Shadow Moire
—— Dial Measurement

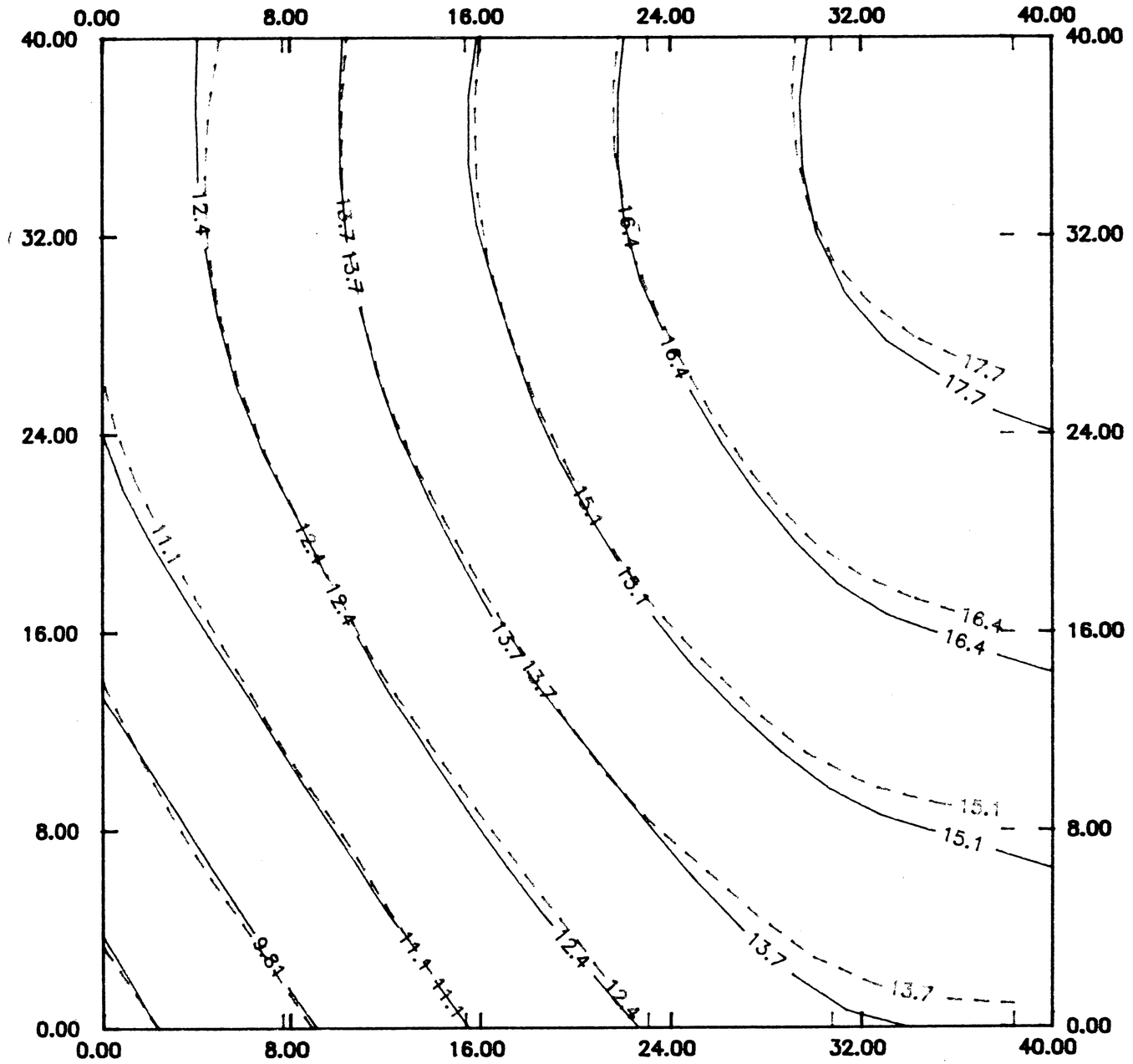

Fig(6 7) Specimen 1, Density 20 l./in.

—— Shadow Moire

—— Dial Measurement

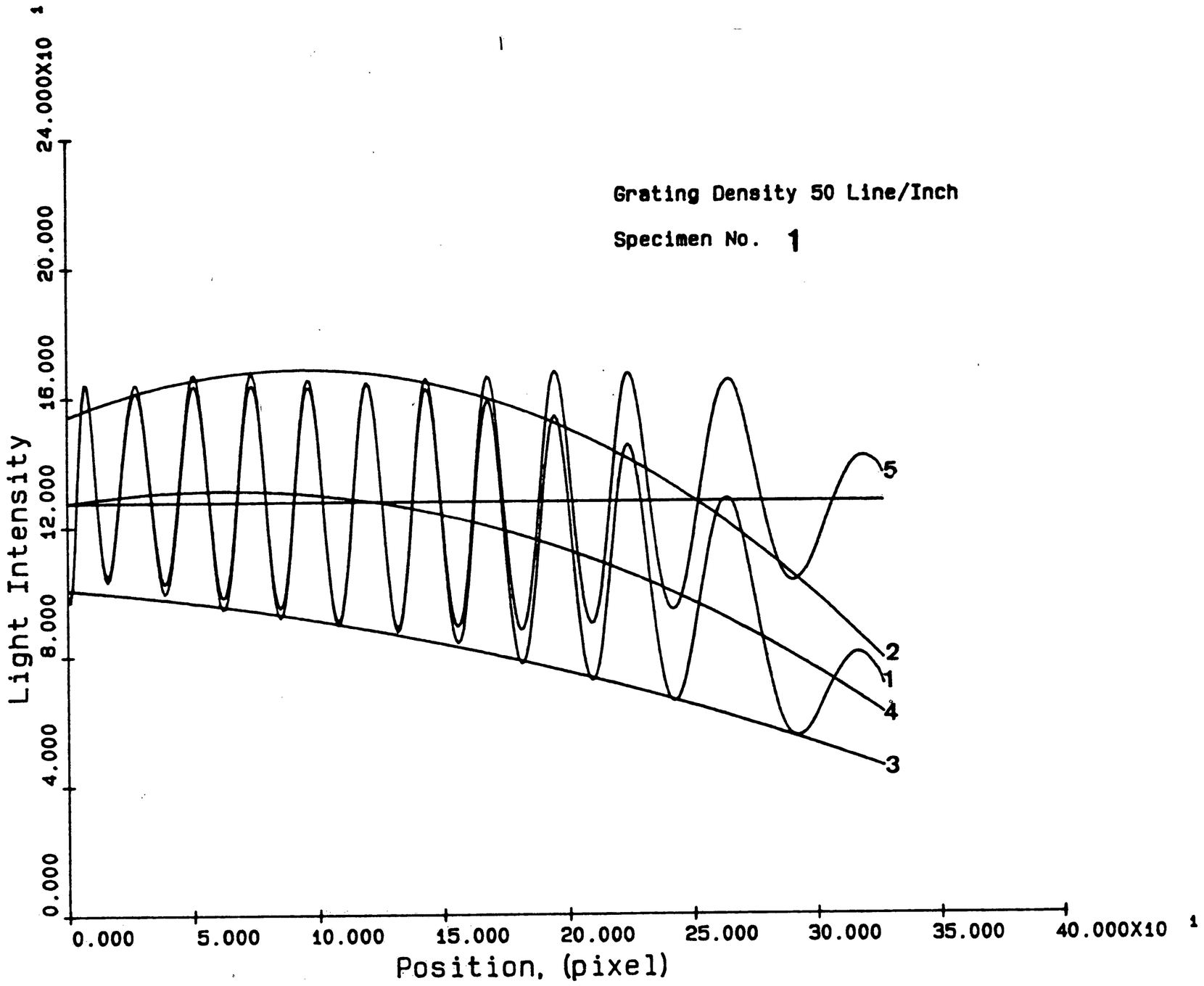

Fig.(6 8 Light Intensity Scan And Modification for Non - Uniform Light Intensity

1 - Original light intensity
2 - Curve-fit for bright fringes
3 - Curve-fit for dark fringes
4 - Mean light intensity (between 2 and 3)
5, - Light intensity after shift

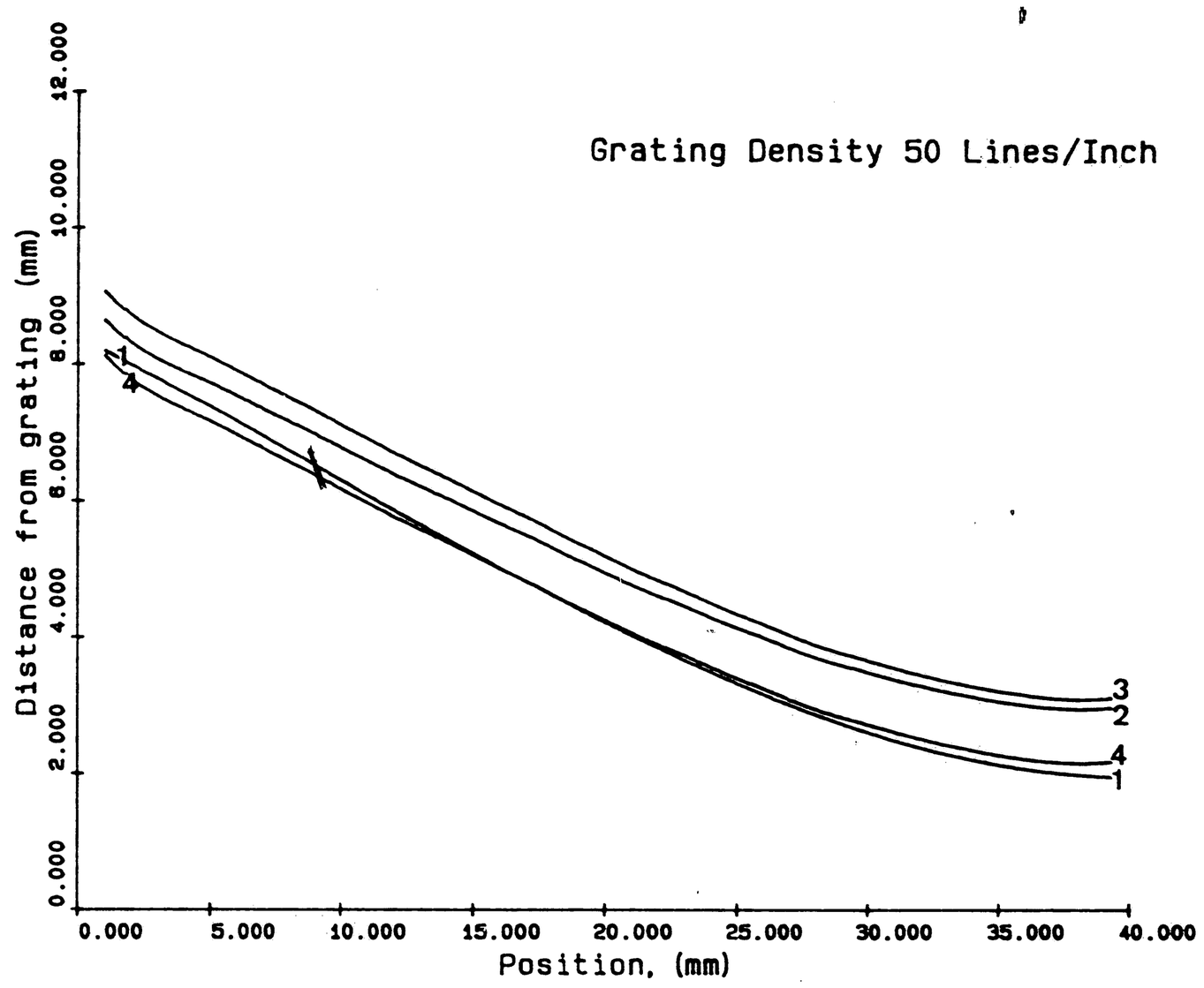

Fig. **6 9** Distance from the grating along the cross-section D-D for specimen 1

1 - Actual depth measured by dial gage
2 - Distance calculated from shadow moire pattern
3 - Distance calculated from shadow moire pattern without taking into account correct angle of light incidence
4 - Distance after shift

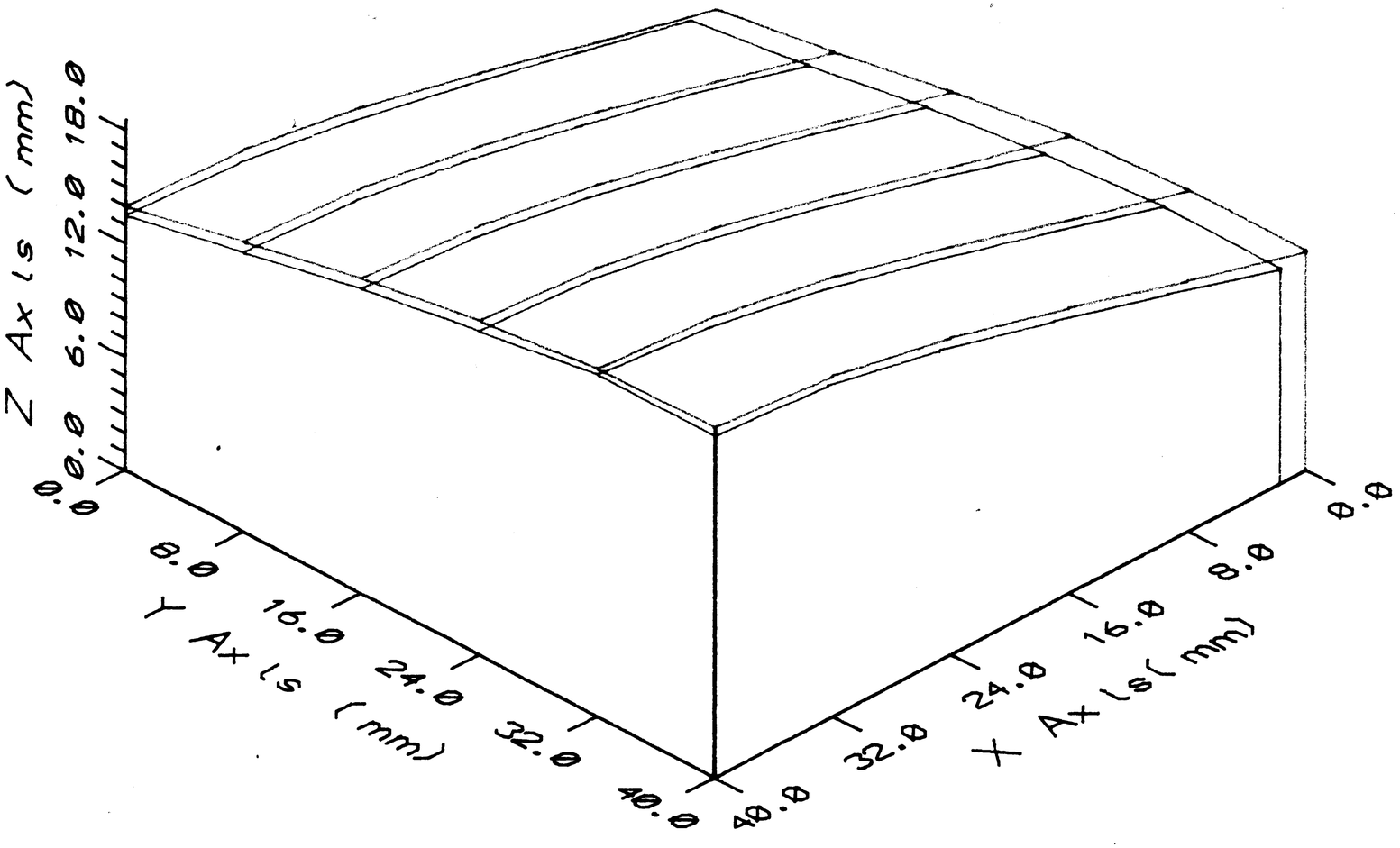

Fig(6 10) Specimen 1, Density 50 l./in.(45 Degree)

—— Shadow Moire
—— Dial Measurement

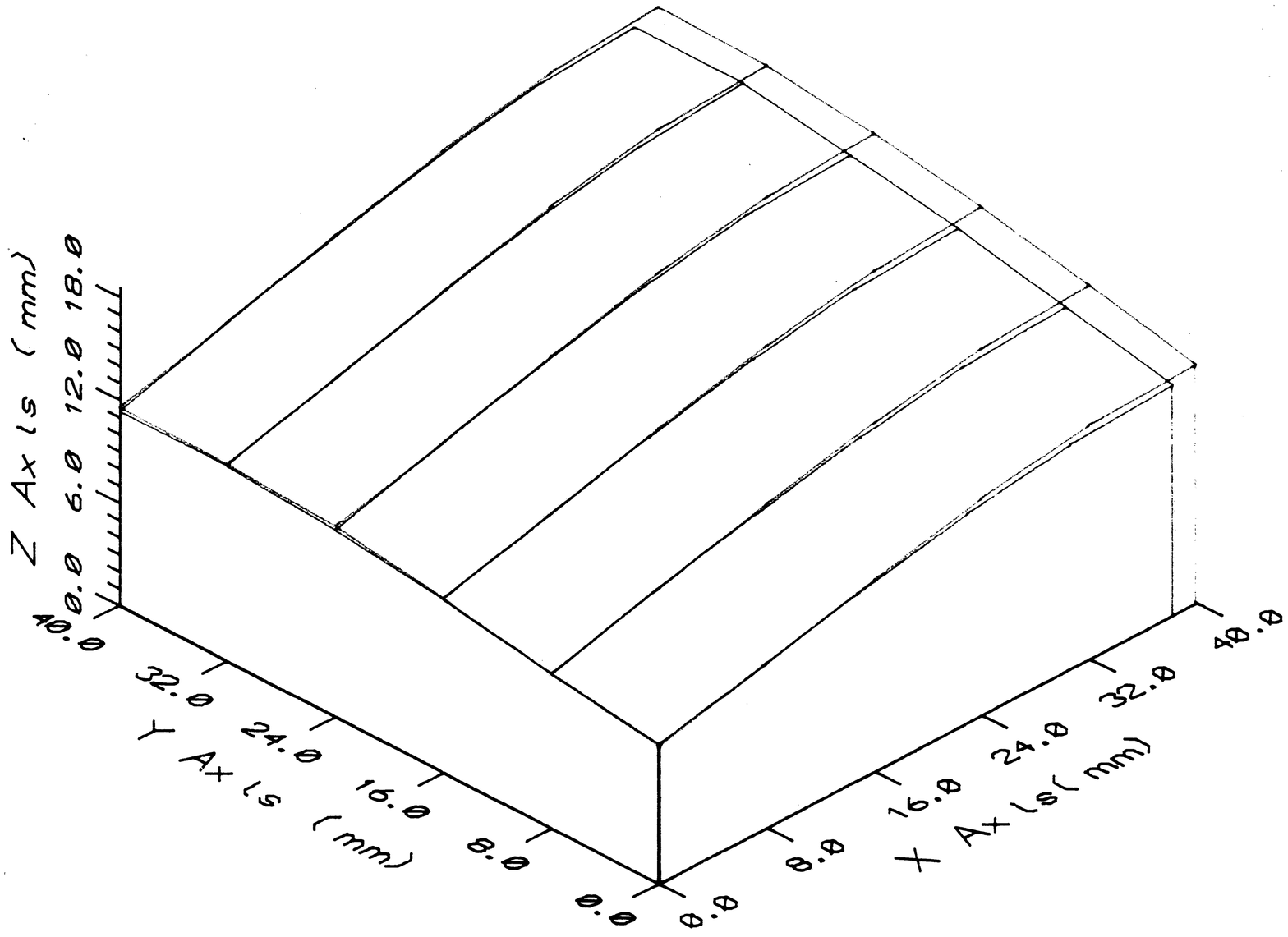

Fig(6 11) Specimen 1, Density 50 l./in.(225 Degree)

—— Shadow Moire
—— Dial Measurement

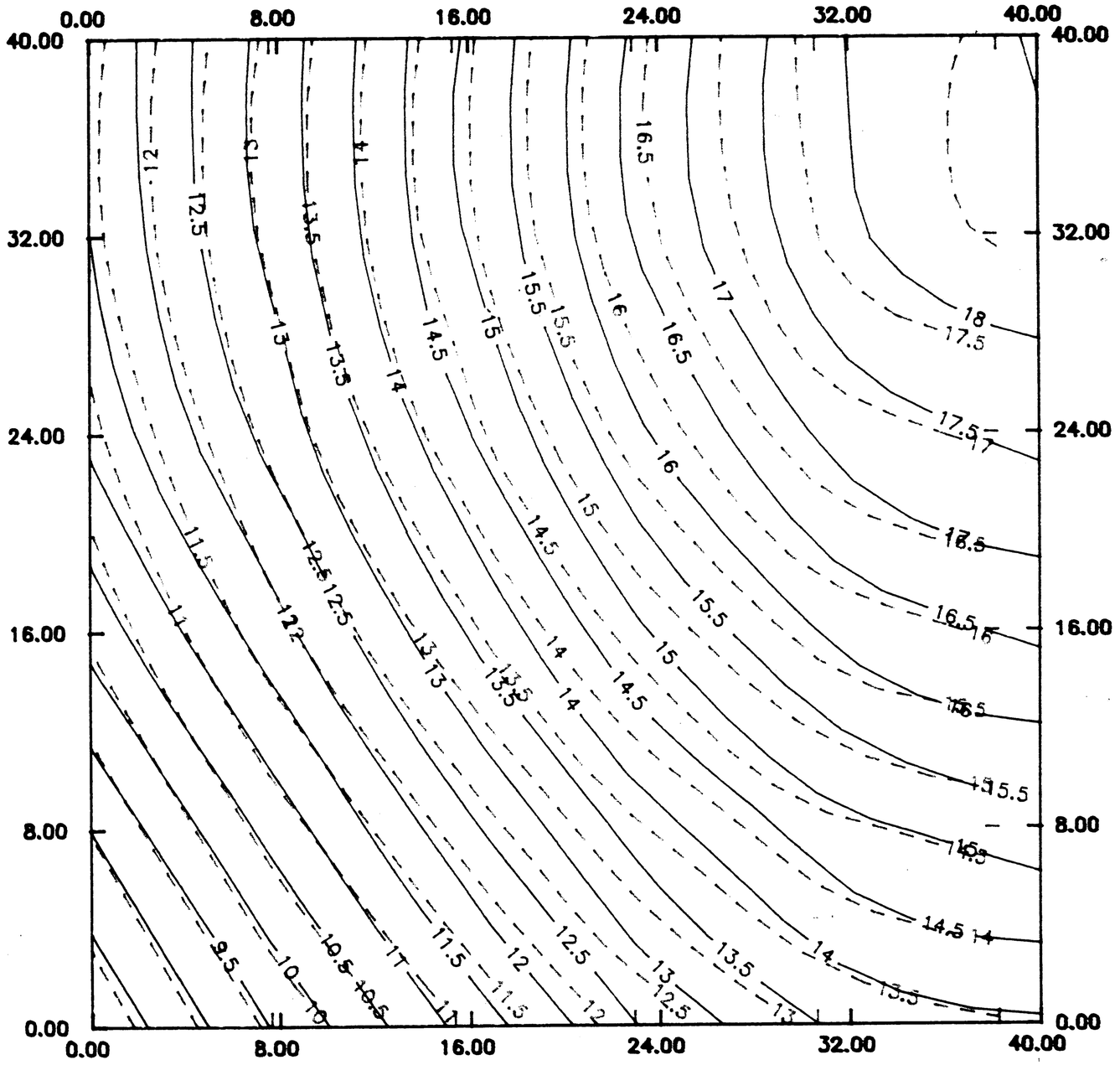

Fig(6 12) Specimen 1, Density 50 l./in.

—— Shadow Moire
—— Dial Measurement

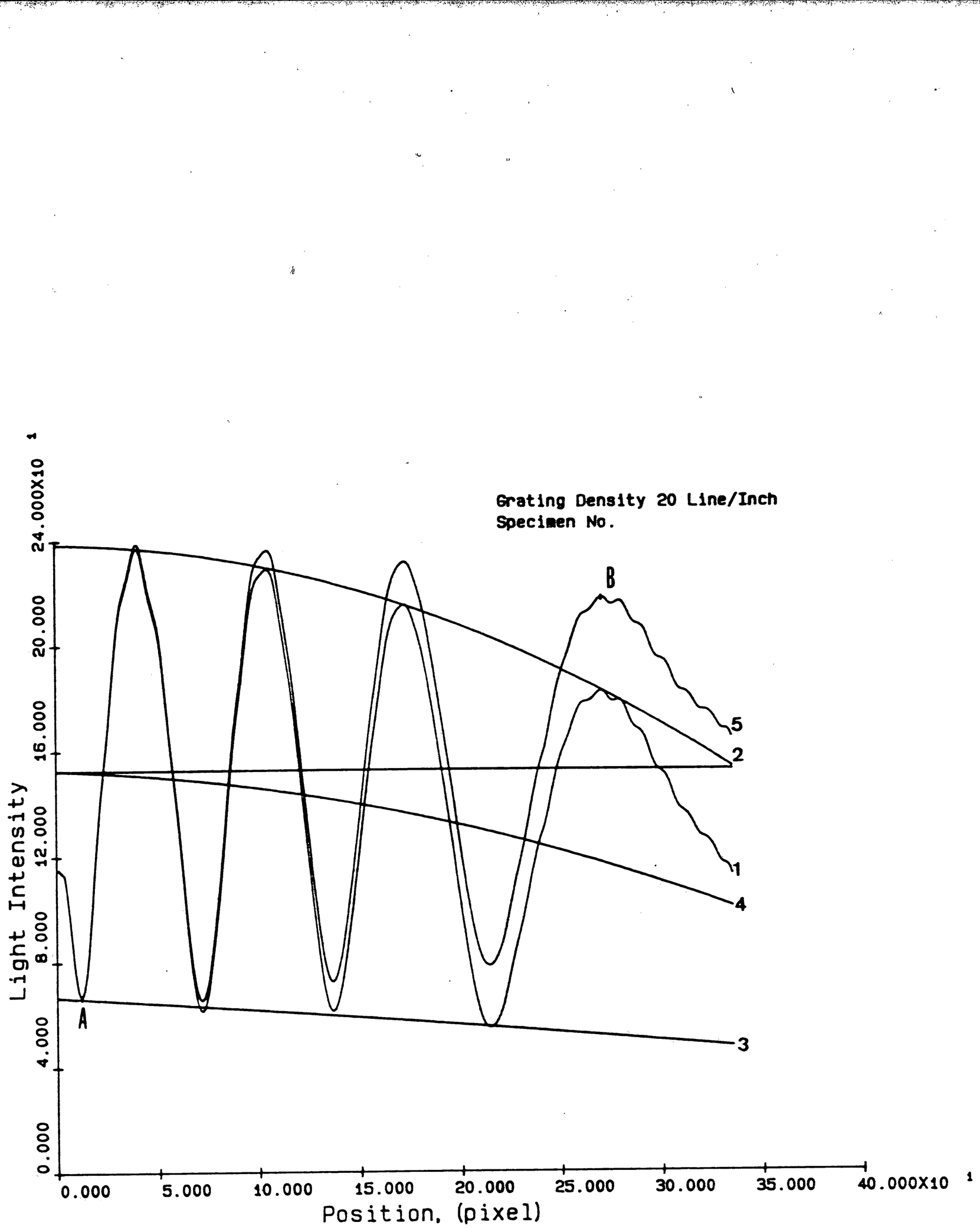

Fig**6 1 3**) Light Intensity Scan And Modification for Non - Uniform Light Intensity

1 - Original light intensity
2 - Curve-fit for bright fring
3 - Curve-fit for dark fringes
4 - Mean light intensity (between 2 and 3)
5 - Light intensity after shift

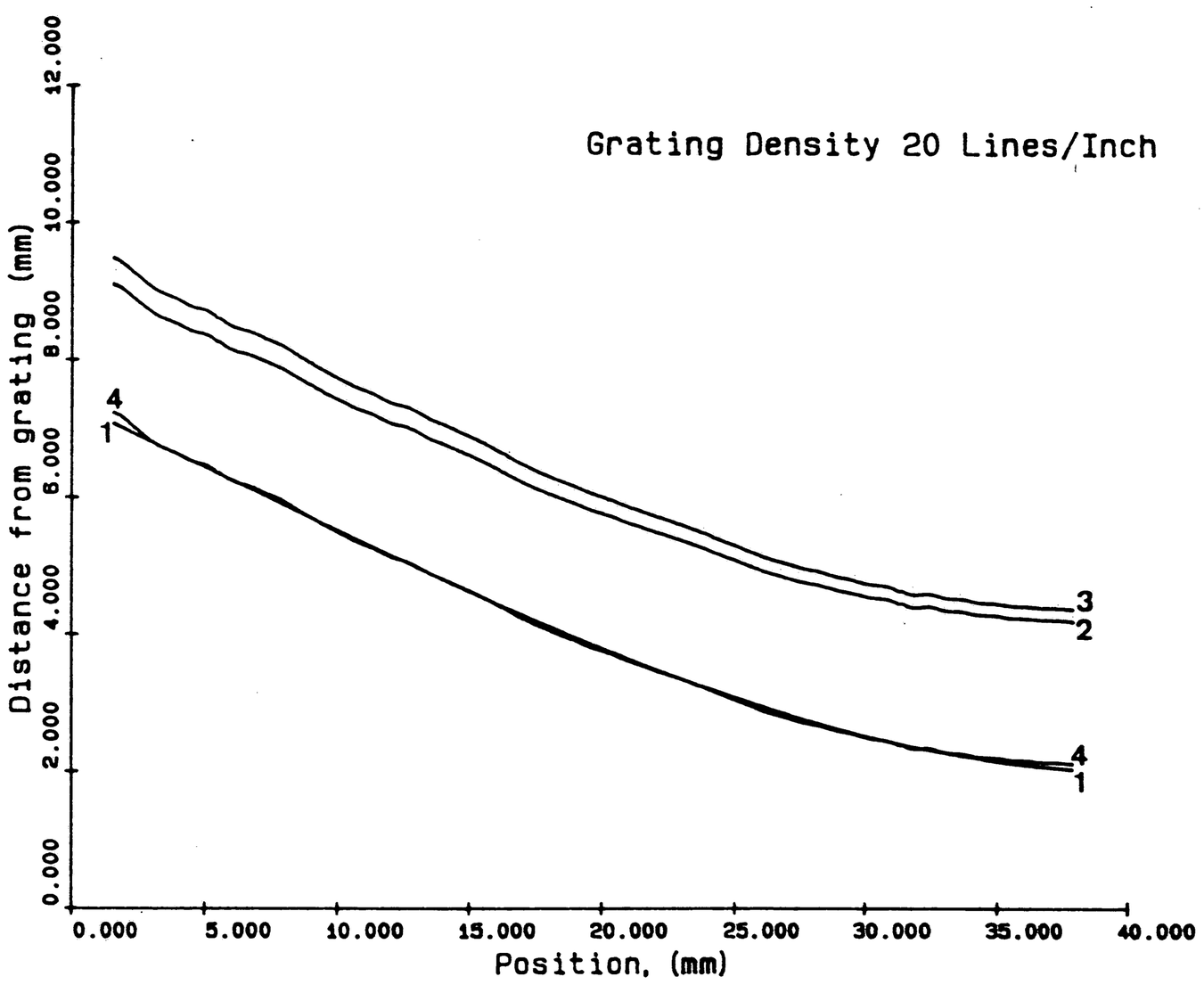

Fig. 6 14 Distance from the grating along the cross-section D-D for specimen 2

1 - Actual depth measured by dial gage
2 - Distance calculated from shadow moire pattern
3 - Distance calculated from shadow moire pattern taking into account correct angle of light incidence
4 - Distance after shift

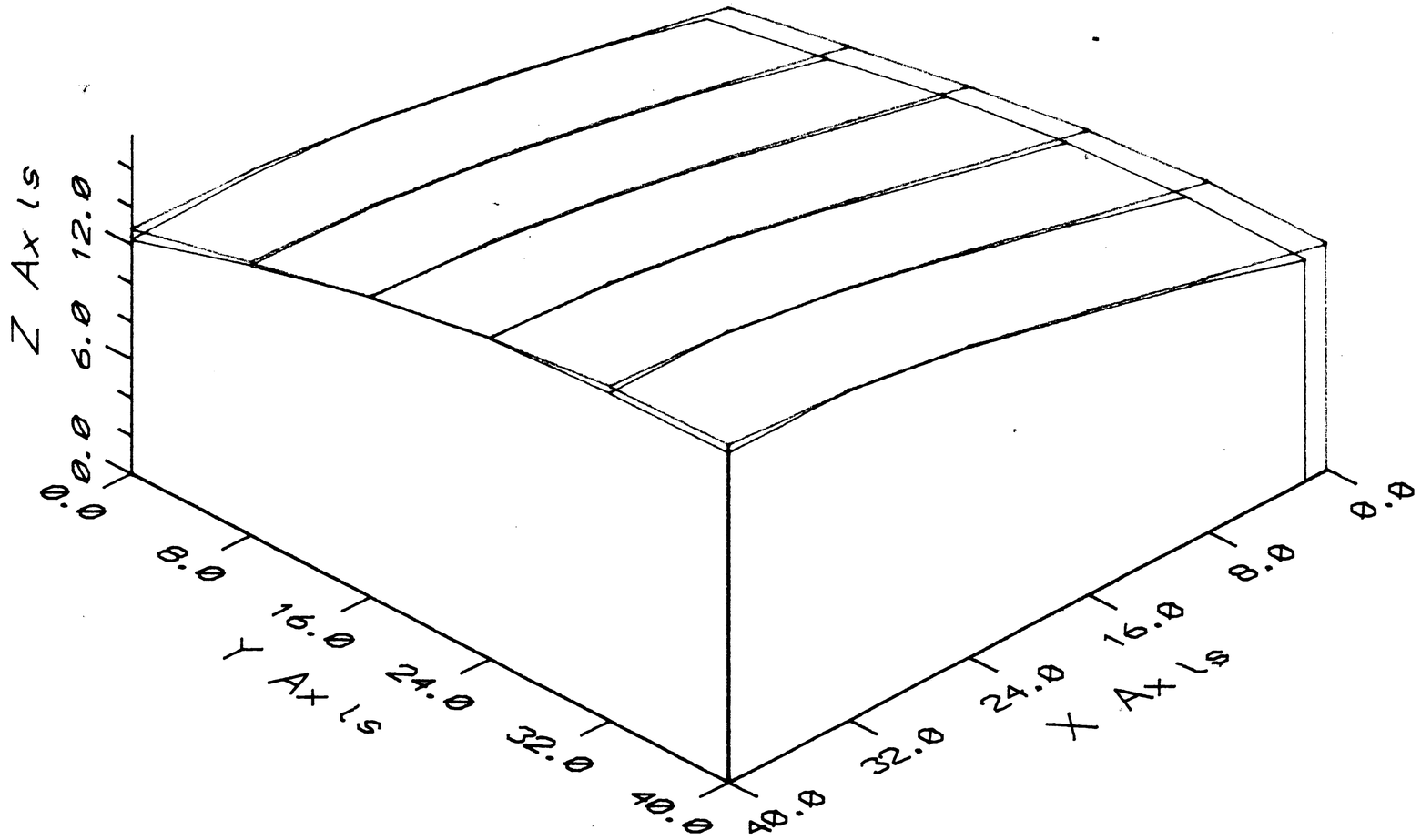

Fig(6.15) Specimen 2, Density 20 l./in. (45 Degree)

—— Shadow Moire
—— Dial Measurement

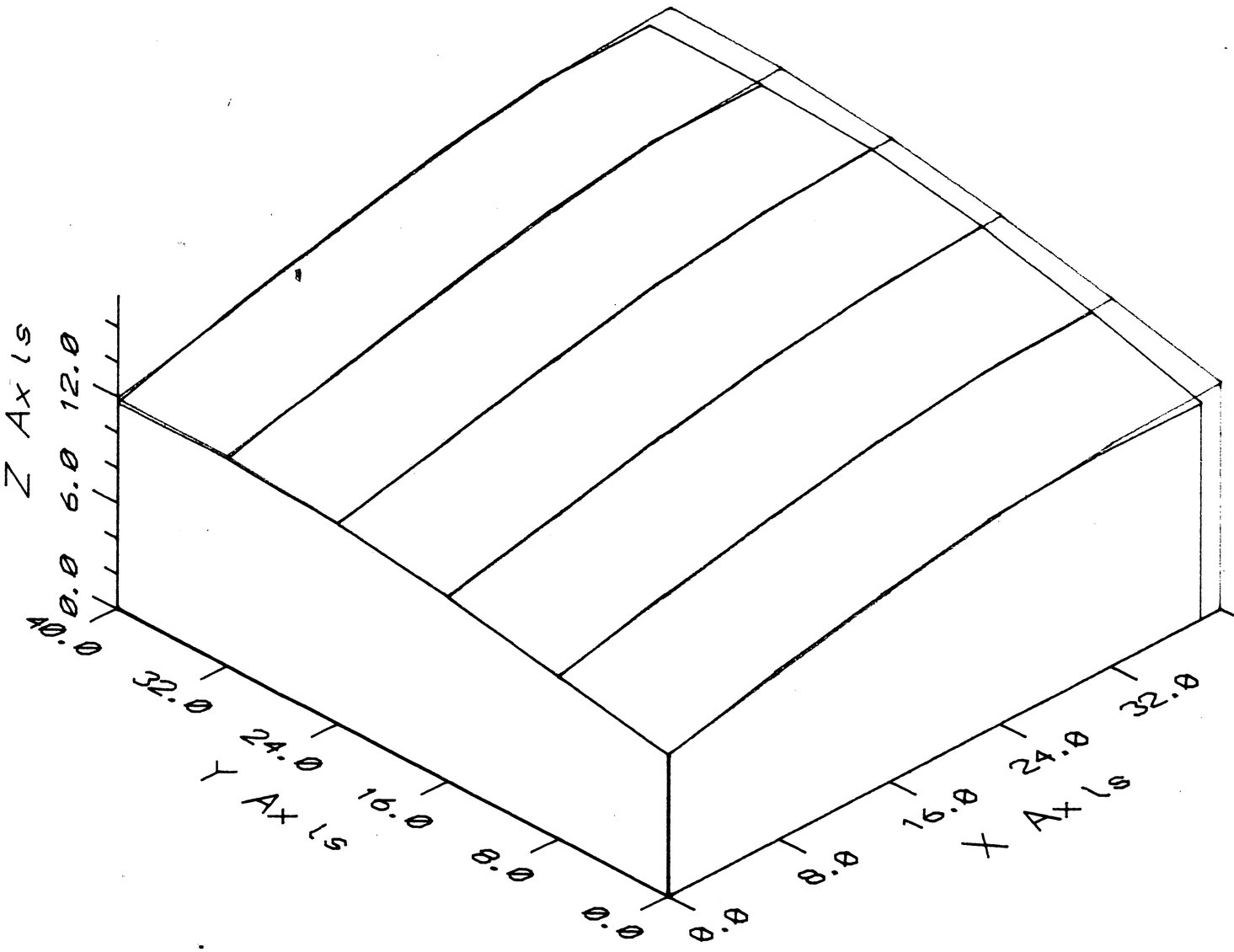

Fig(6 16) Specimen 2, Density 20 l./in. (225 Degree)

—— Shadow Moire
—— Dial Measurement

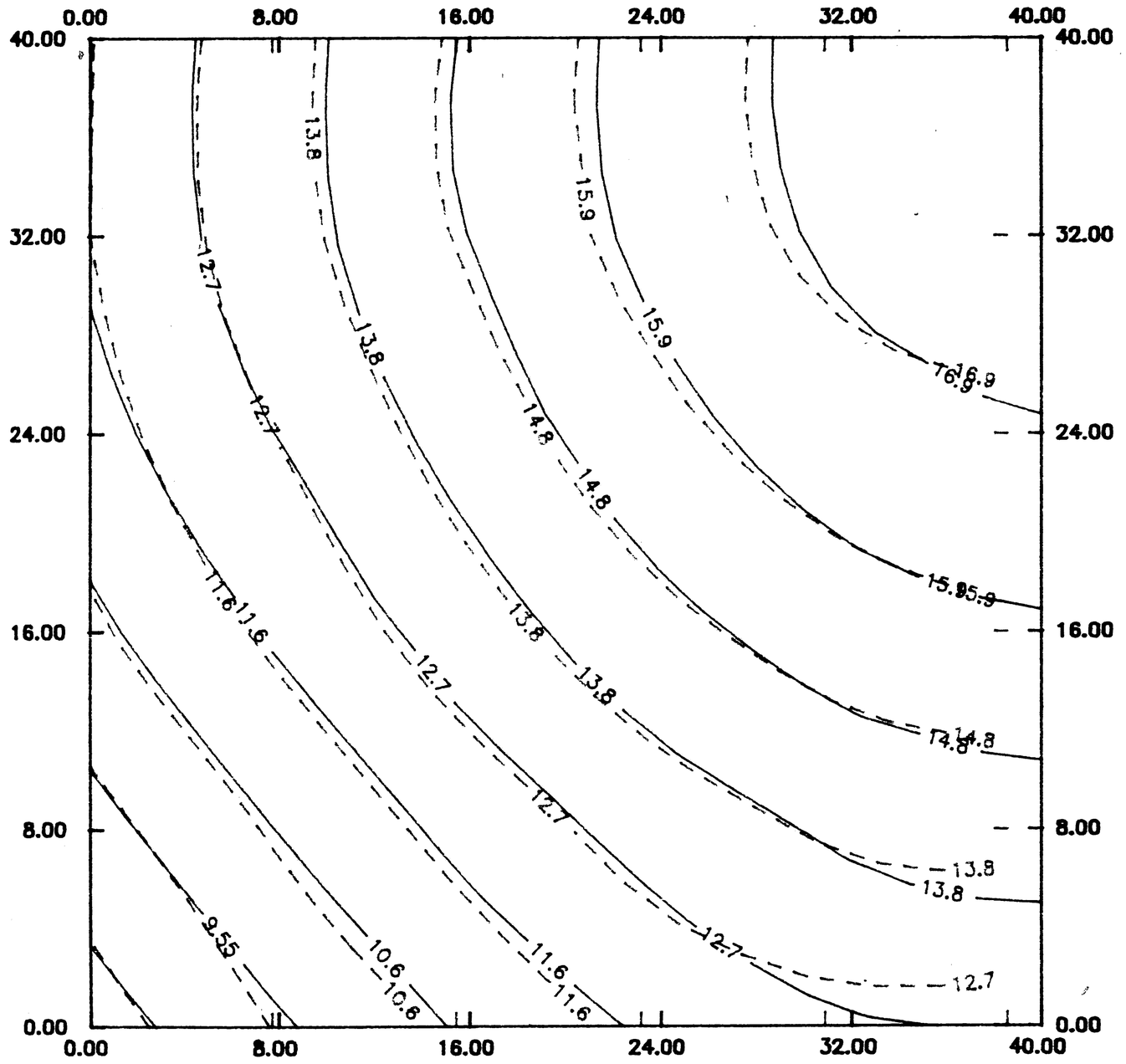

Fig(6 17) Specimen 2, Density 20 l./in.

—— Shadow Moire
—— Dial Measurement

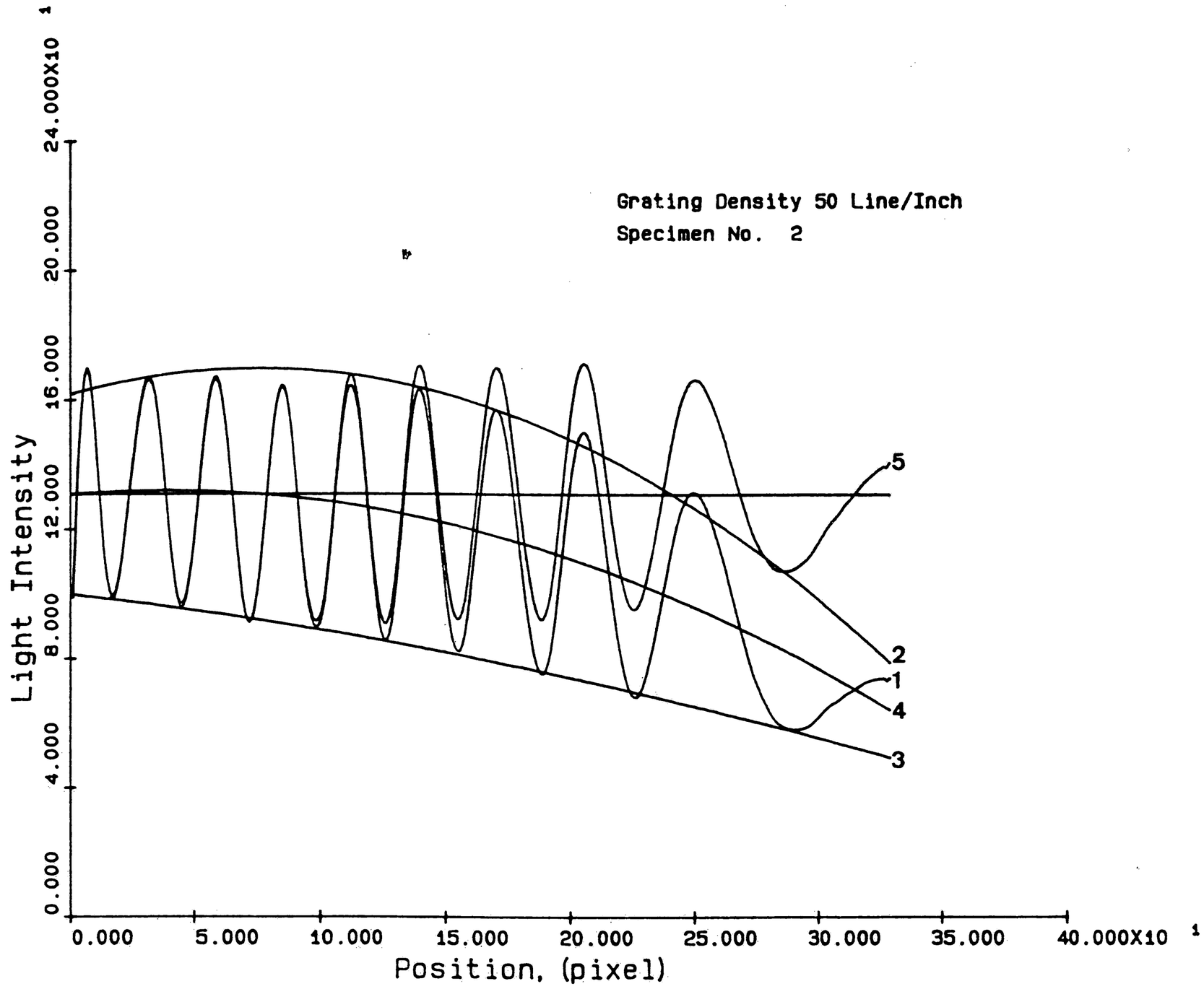

Fig.**6 18** Light Intensity Scan And Modification for Non - Uniform Light Intensity

1 - Original light intensity
2 - Curve-fit for bright fringes
3 - Curve-fit for dark fringes
4 - Mean light intensity (between 2 and 3)
5 - Light intensity after shift

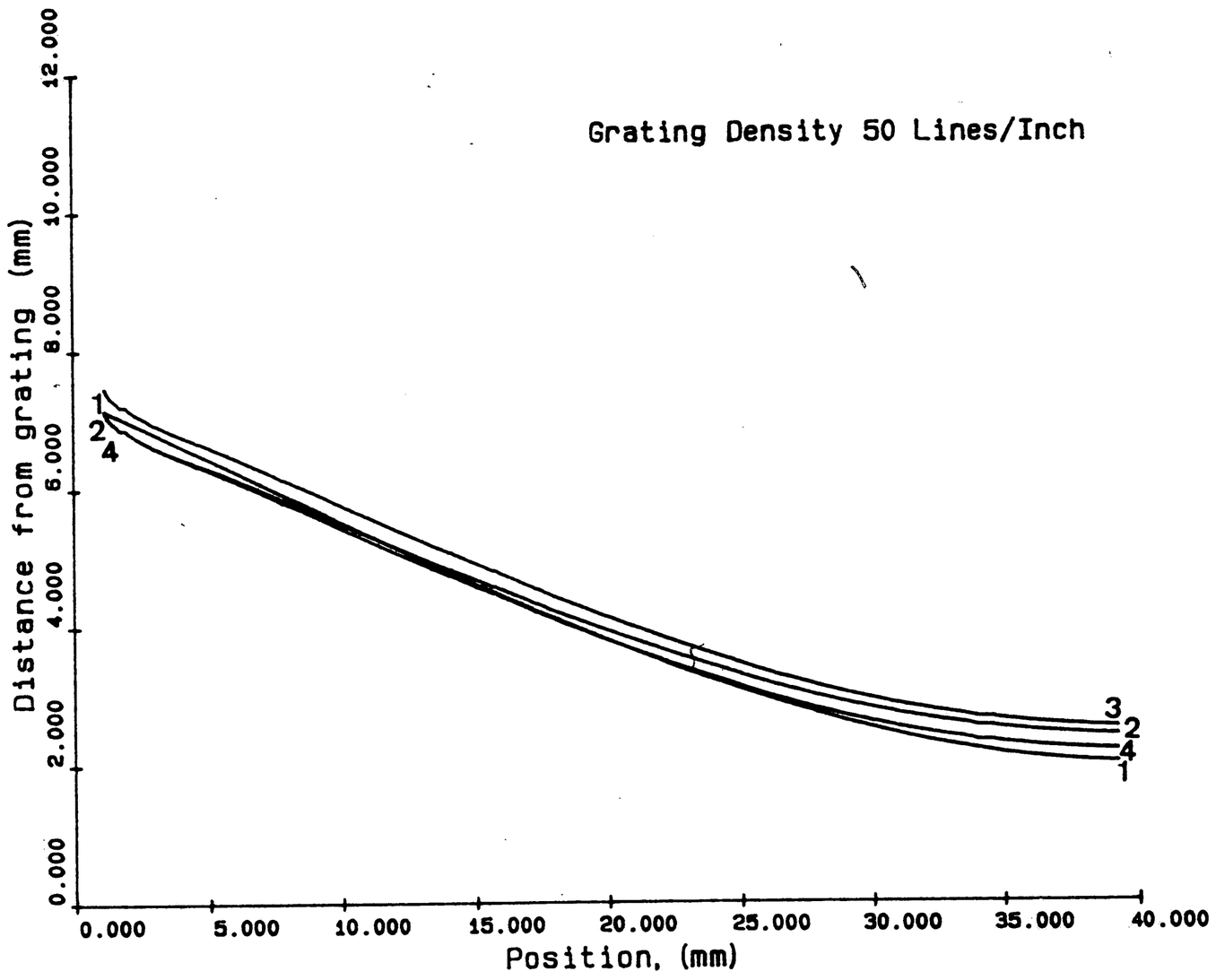

Fig. **6 19** Distance from the grating along the cross-section D-D for specimen 2

1 - Actual depth measured by dial gage
2 - Distance calculated from shadow moire pattern
3 - Distance calculated from shadow moire pattern taking into account correct angle of light incidence
4 - Distance after shift

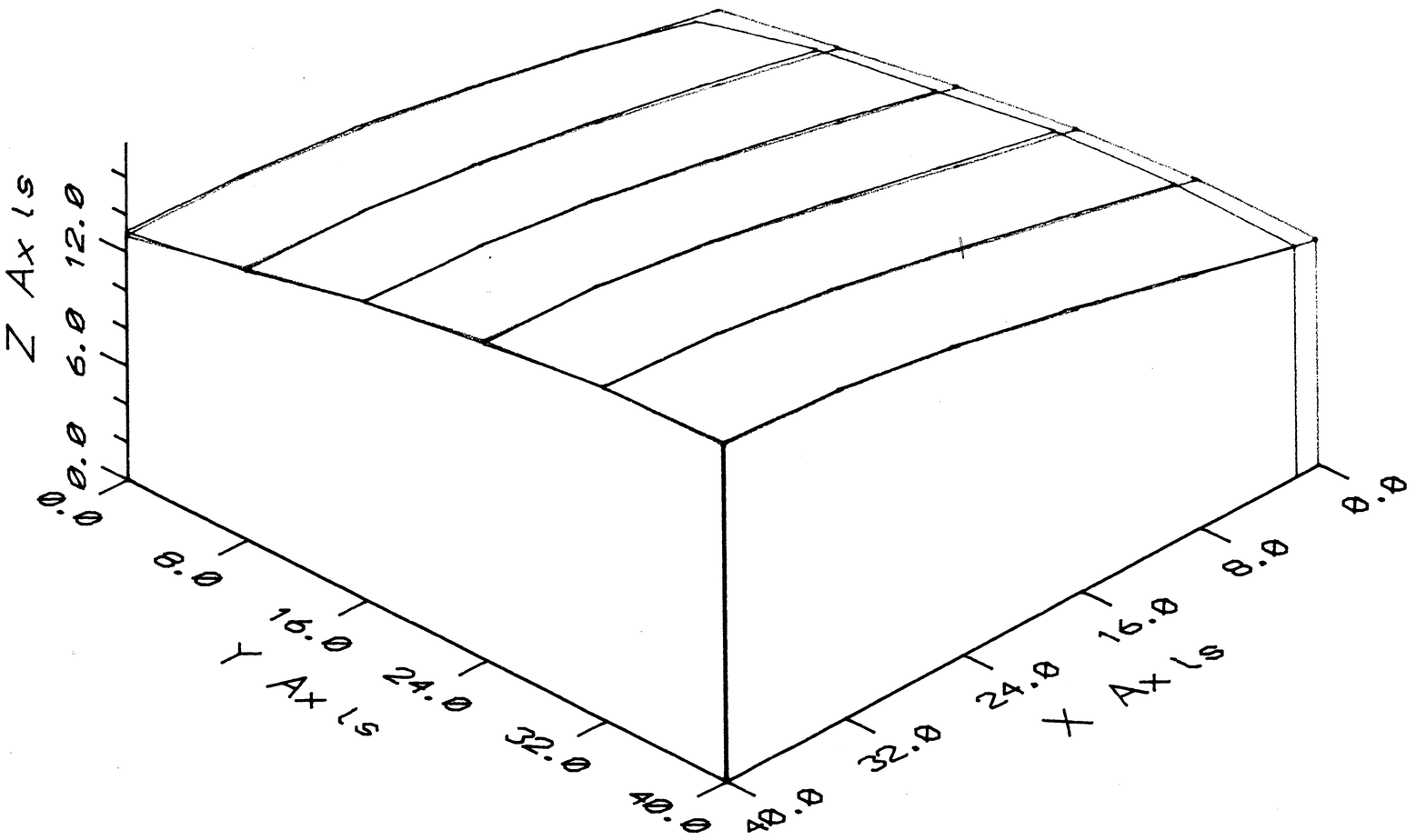

Fig(6 20) Specimen 2, Density 50 l./in. (45 Degree)

——— Shadow Moire
— — — Dial Measurement

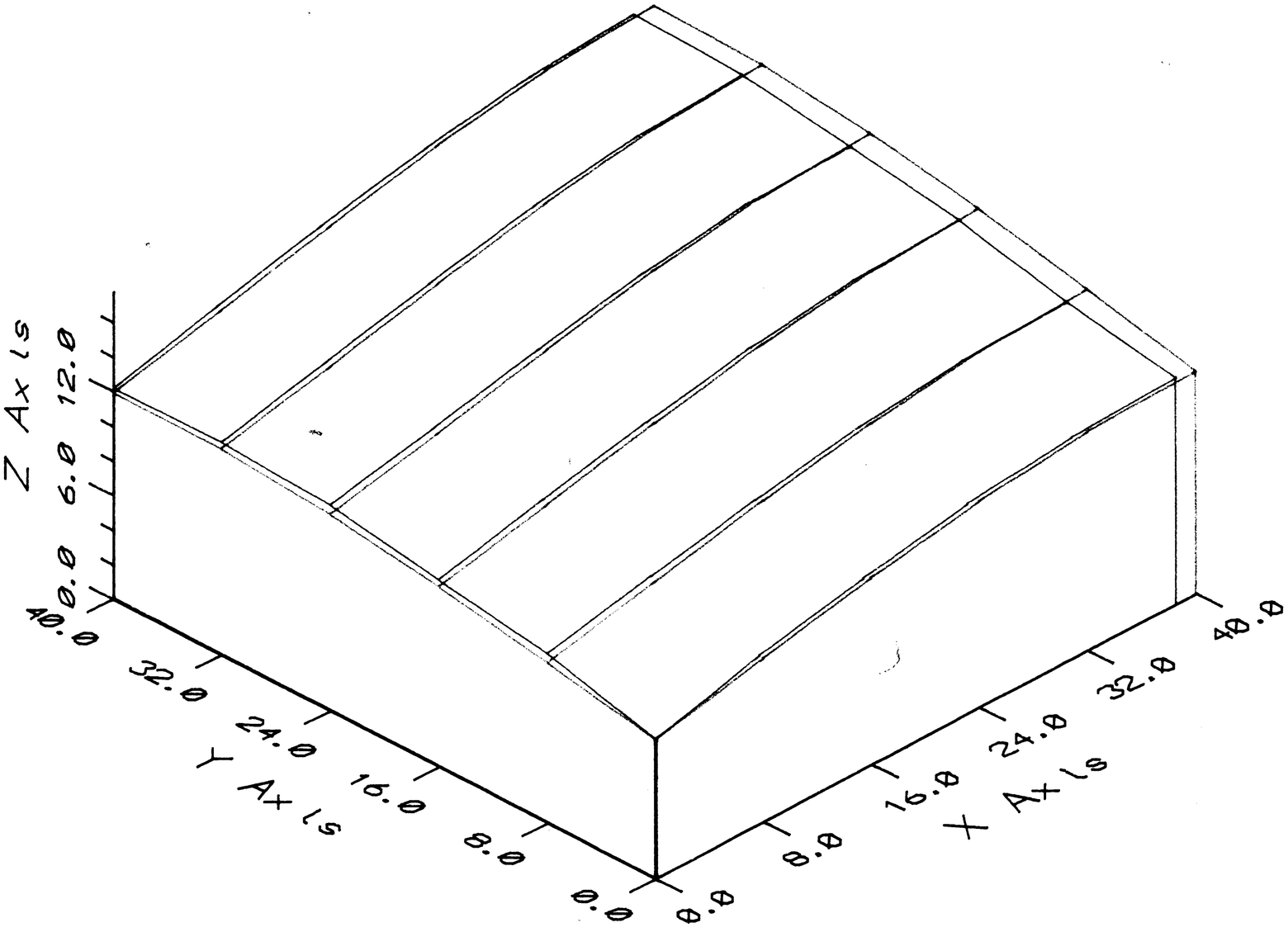

Fig(6.21) Specimen 2, Density 50 l./in. (225 Degree)

——— Shadow Moire
——— Dial Measurement

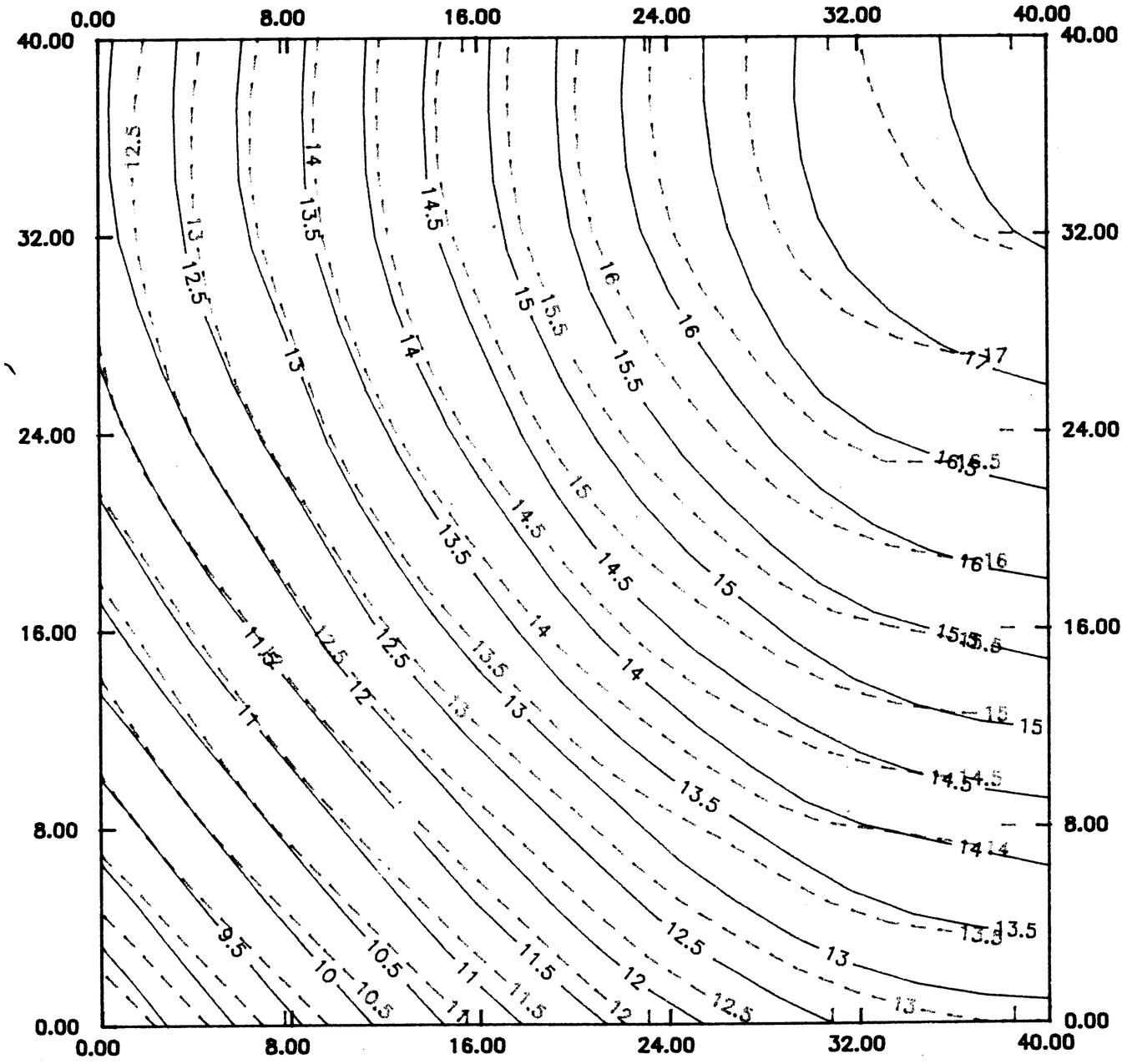

Fig(6 2 2) Specimen 2 Density 50 l./in.

—— Shadow Moire
—— Dial Measurement

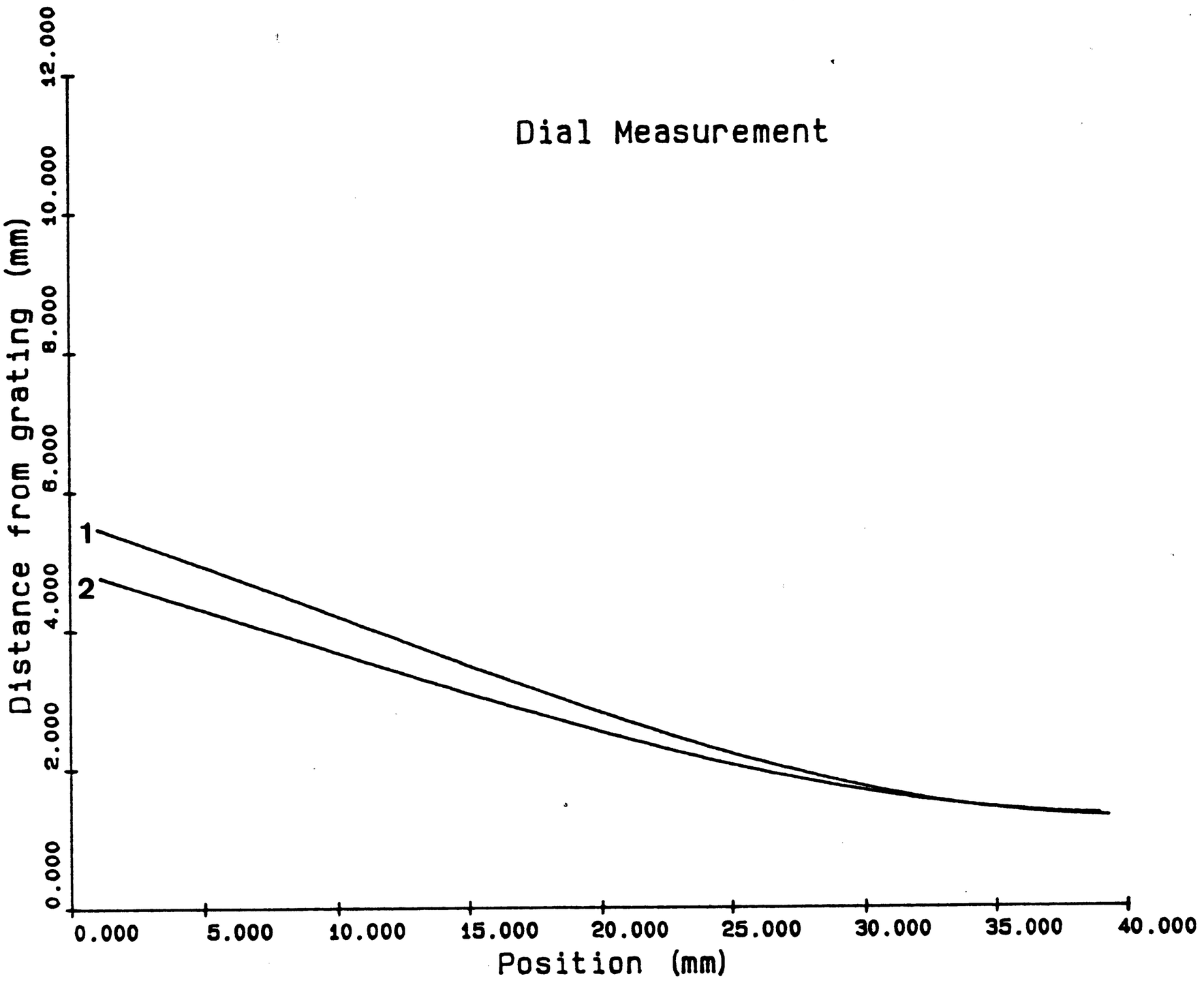

Fig. (6 23) Distance from the grating along the scan line

1. Specimen 1
2. Specimen 2

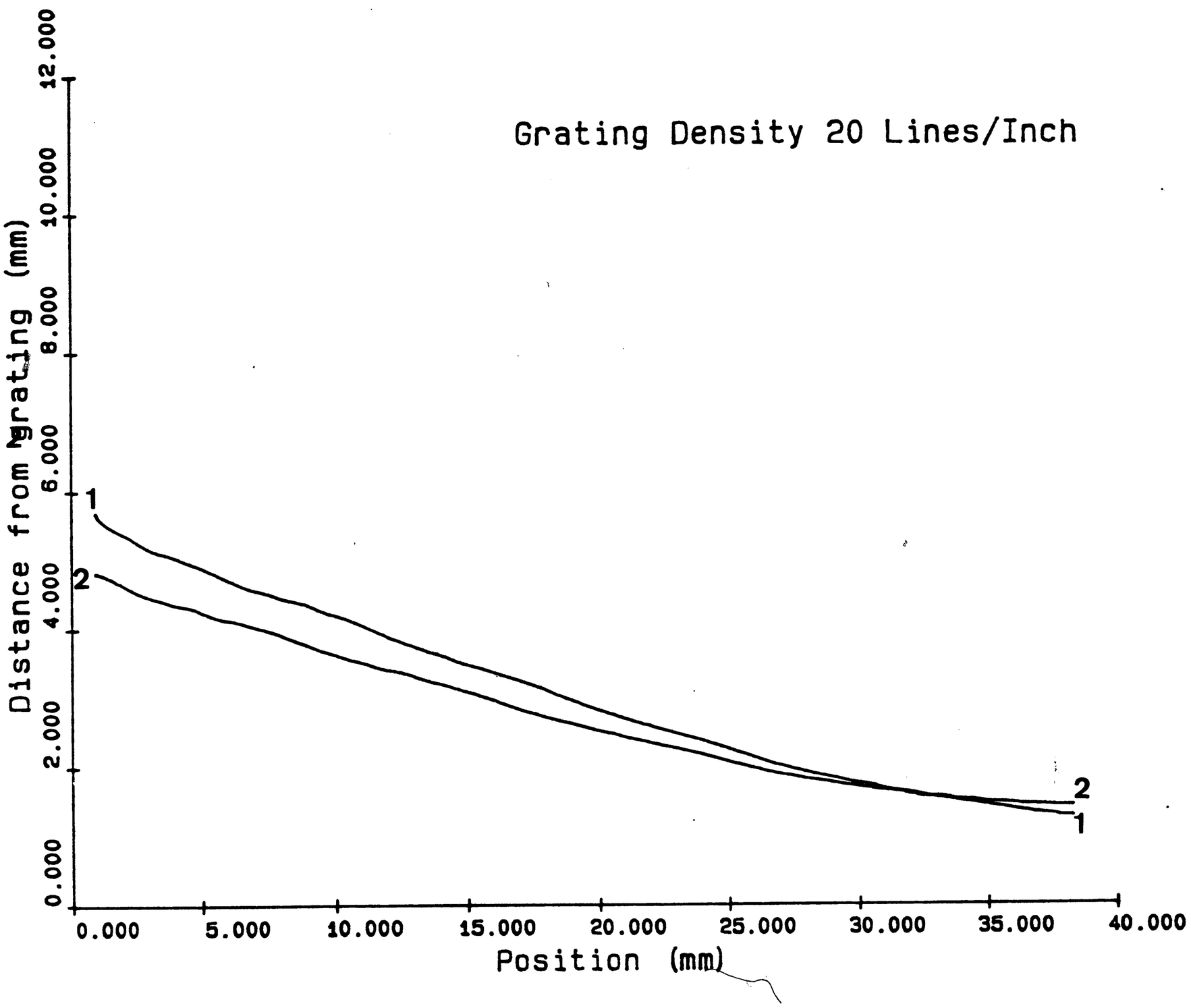

Fig. (6 24 Distance from the grating along the scan line

1. Specimen 1
2. Specimen 2

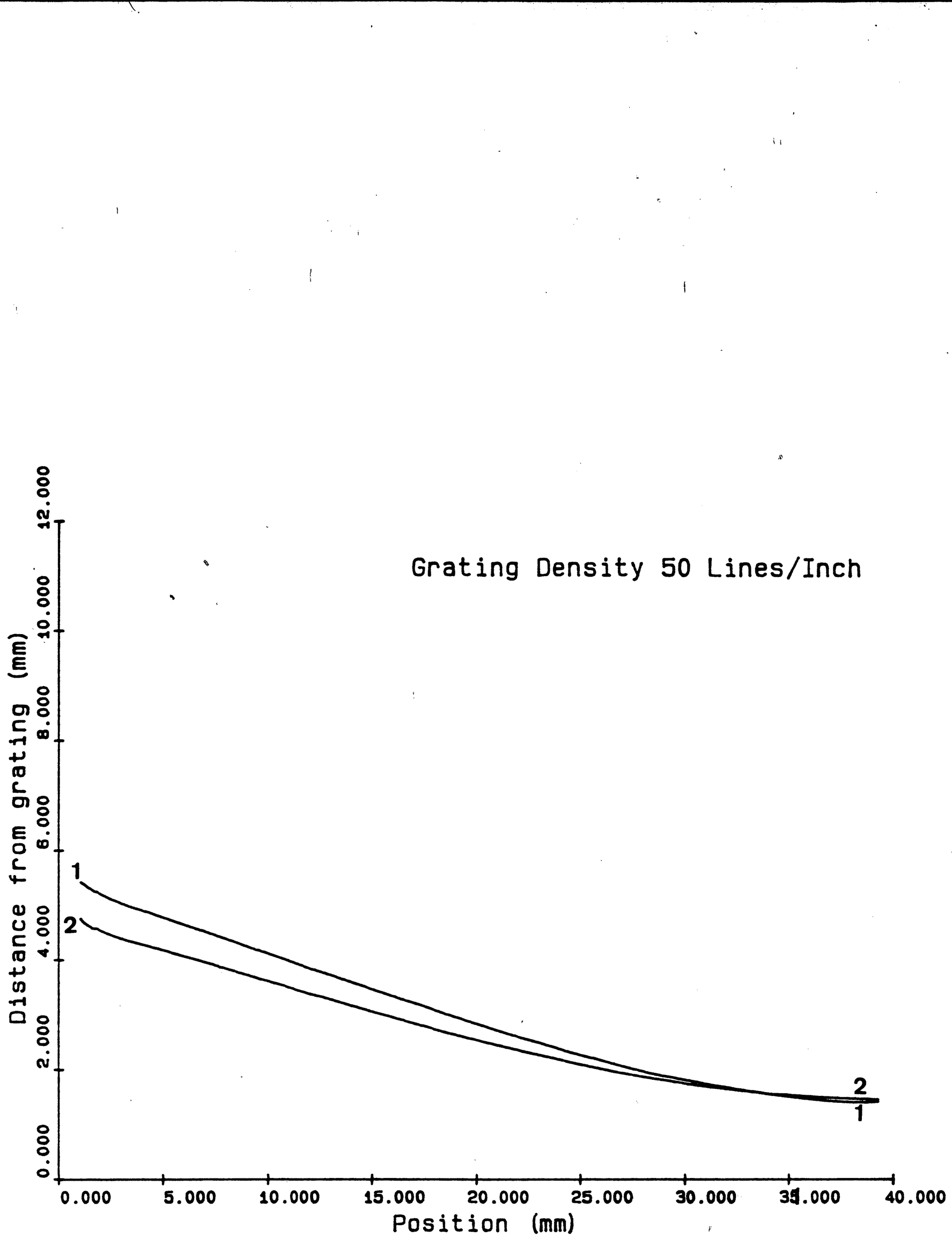

Fig. (6 25) Distance from the grating along the scan line

1. Specimen 1
2. Specimen 2

7.DISCUSSION

In order to achieve a high accuracy of the out-of-plane displacement measurements, several important factors have to be taken into account. In this chapter the effects of non-uniform light field, investigate the correct angle between light source and camera, as well as calculation at the non-half fringe area are discussed.

A. Non-uniformity of light field

In figure 6.3,6.8,6.13,6.18 (curve 1) the resulting light field is highly non-uniform, this was because the collimated light source is located at an angle θ with respect to the master grating and camera[figure 3.1]. The result may not create any problem in the classical version of the shadow moire where only locations of the full fringe order are of interest. Here, one has to account for the non-uniformity of the light field.

The specimen was positioned as close as possible in front of the master grating and illuminated by the same light source. The resulting light intensity was scanned along a horizontal cross-section.

Figure 6.3, curve 1, represents the original light intensity distribution. Locations of bright (curve 2) and dark (curve 3) fringe are approximated by a second order polynomial.

Various possibilities were investigated before it was concluded that a second order curve is sufficient to represent the light field non-uniformity.

The average light intensity can be described as :

$$AVEC(X) = ((BC(X)-DC(X))/2)+BC(X) \quad \ldots\ldots(7.1)$$

where

x - array index of pixel element along the scan line

AVEC(X) - The average light intensity curve between curve 2 and curve 3.

BC(x) - Bright-fringe peak curve

DC(x) - Dark-fringe peak curve

One can introduce a correction factor CF(x):

$$CF(x) = ABS(AVEX - AVEC(x)) \quad \ldots\ldots (7.2)$$

where

AVEX - The maximum value of the average light intensity curve (Fig. 6.3, curve 4)

This factor was derived for each cross - section. It was applied to the acquired light intensity at the scan cross-section. The modified light intensity LM(x) was calculated as :

$$LM(x) = LO(x) + CF(x) \quad \ldots\ldots\ldots\ldots (7.3)$$

where

LO(x) - The original light intensity curve

The result of the modification was a curve that exhibited less variation in the light intensity than the original data(figure 6.3, curve 5). Taking into account the non-uniformity of light field improved the accuracy by only 0.2 percent for the specimen under investigation.

B. Determination of the correct angle of light incidence

A correction coefficient to investigate the actual value of angle θ [chapter 2] was calculated and introduced in this section. A calibration wedge with known slope was built and used for calculating the correction coefficient. The results were modified using the correction coefficient to correct the geometrical inconsistency of the experimental set-up. The correction coefficient is expressed as

$$\text{Correction Coefficient} = \frac{\text{Calculated slope}}{\text{Measured slope}} \quad \ldots (7.4)$$

The calculated distance [figures 7.2,7.3, curve 2] was obtained from the shadow moire pattern[figure 7.1] of a calibration wedge with the known slope. The shadow moire pattern was recorded from the grating of 0.508 mm/L and 1.27 mm/L. The measured distance[figures 7.2,7.3 curve 1] was obtained by measuring the actual depth of the calibration wedge.

Figures 7.4 and 7.5 depict the relation between calculated and measured distances. The corresponding correction coefficients(eq. 7.4) were 1.042 and 1.049, or equivalently θ = 46.18 and 46.37 degrees respectively.

In figures 7.2 and 7.3 the gap between the curve 1 and curve 2 was resulted from the inaccuracy in the integer fringe assignment (Figure 7.1), however it did not influence the correction coefficient, since only slope was measured. In figures 7.2 and 7.3 curve 3 represented the result of curve 2 multiplied by the above correction coefficient, and it showed significantly increased accuracies of 1.2 and 1.4 percent respectively. Thus, this correction coefficient can also provide an accurate modification for the displacement field of the other specimen if the experimental set-up remains unchanged.

C. Calculation of the out-of-plane displacement in the non-half fringe area

The non-half fringe area can be observed in figure 6.2(curve 2 - the light intensity curve along the scan line), the maximum and minumum light intensity locations along the curve 2 identify the multiples of half fringe orders. When the first point on the curve does not represent half or full fringe location, the part of the curve between the point and the first minimum or maximum will be identified as a non-half fringe area. Similarly, the region between the last point on the curve which is not full or half fringe and the prceceeding minimum or maximum will be identified as a non-half fringe area. In case when the specimen's surface is monotonic structure, the non-half fringe area usually occurs at the end or the beginning of the scan line. Thus, in order to investigate the displacement field along the specific scan line, a routine was developed to include the non-half fringe areas.

In figure 6.13 two regions of the non-half fringe field are shown along the scan line. On the left hand side this region begins from the peak(location A) on the dark fringe(minimum light intensity) moving left to the beginning of the light intensity curve. On the right hand side this region begins from the peak of the fright fringe(location B) moving right to the end of the light intensity curve. The equation 3.4 was applied to calculate the out-of-plane displacement of non-half fringe area. The amplitude of these two non-half fringe area was selected from the half fringe either before or after the non-half fringe area.

The fringe number for the non-half fringe also refers either to the fringe number before or after the non-half fringe area. Figure 6.14 shows that the result of the calculation is in agreement with the dial gage measurements.

The modifications - effects of non-uniform light field, calibration of correct angle and calculation of non-half fringe area - have been demonstrated in this chapter. The result of taking into account the non-uniform light distribution is relatively insignificant. On the other hand, the calibration for the correct angle significantly improves the experimental data. This improvement can also be obtained by a high precision instrument capable to provide a correct angle set-up between grating and the camera. The calculation of the non-half fringe area can enchance the out-of-plane dispacement data along the scan line near the edge of the specimen.

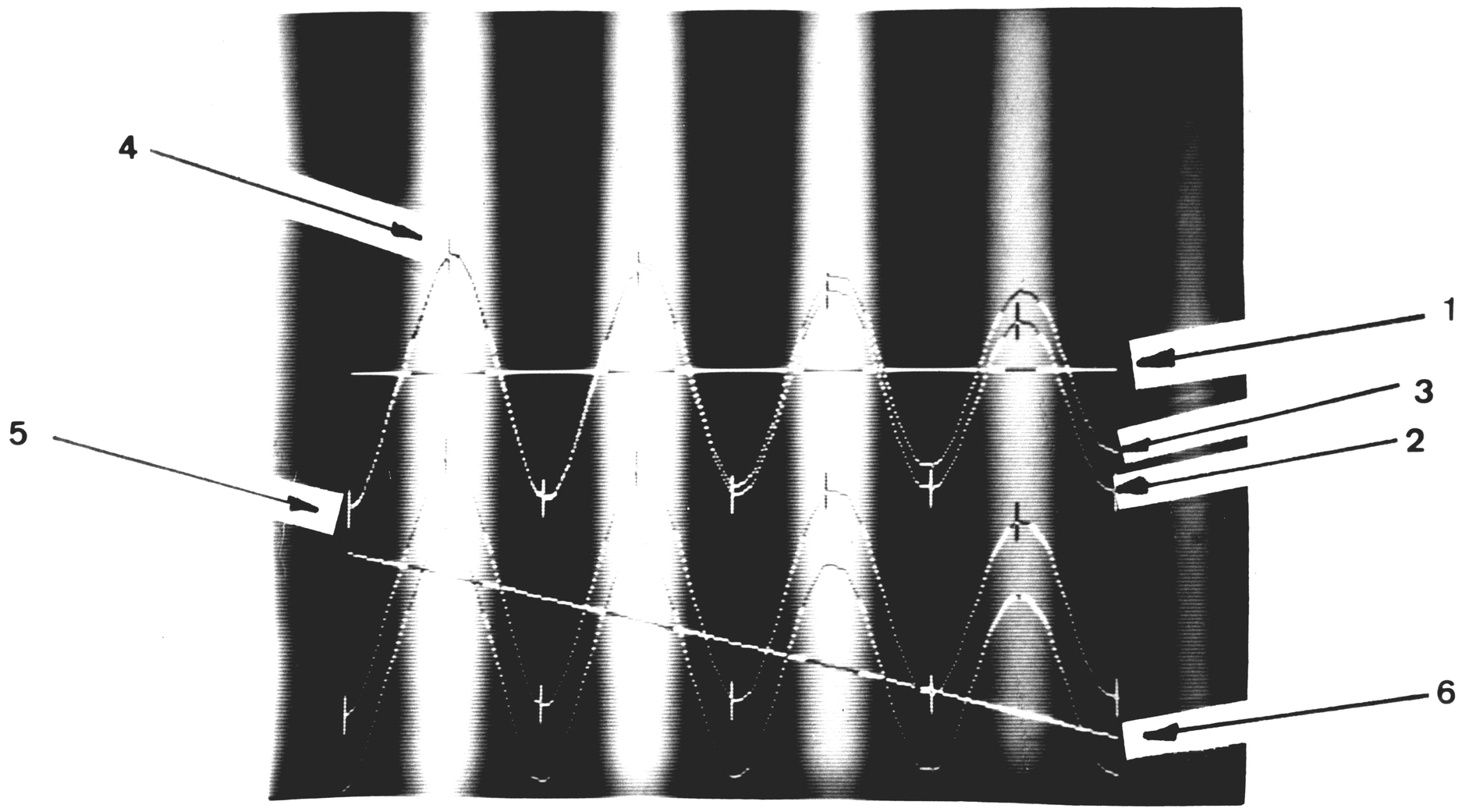

Density 20 lines/inch

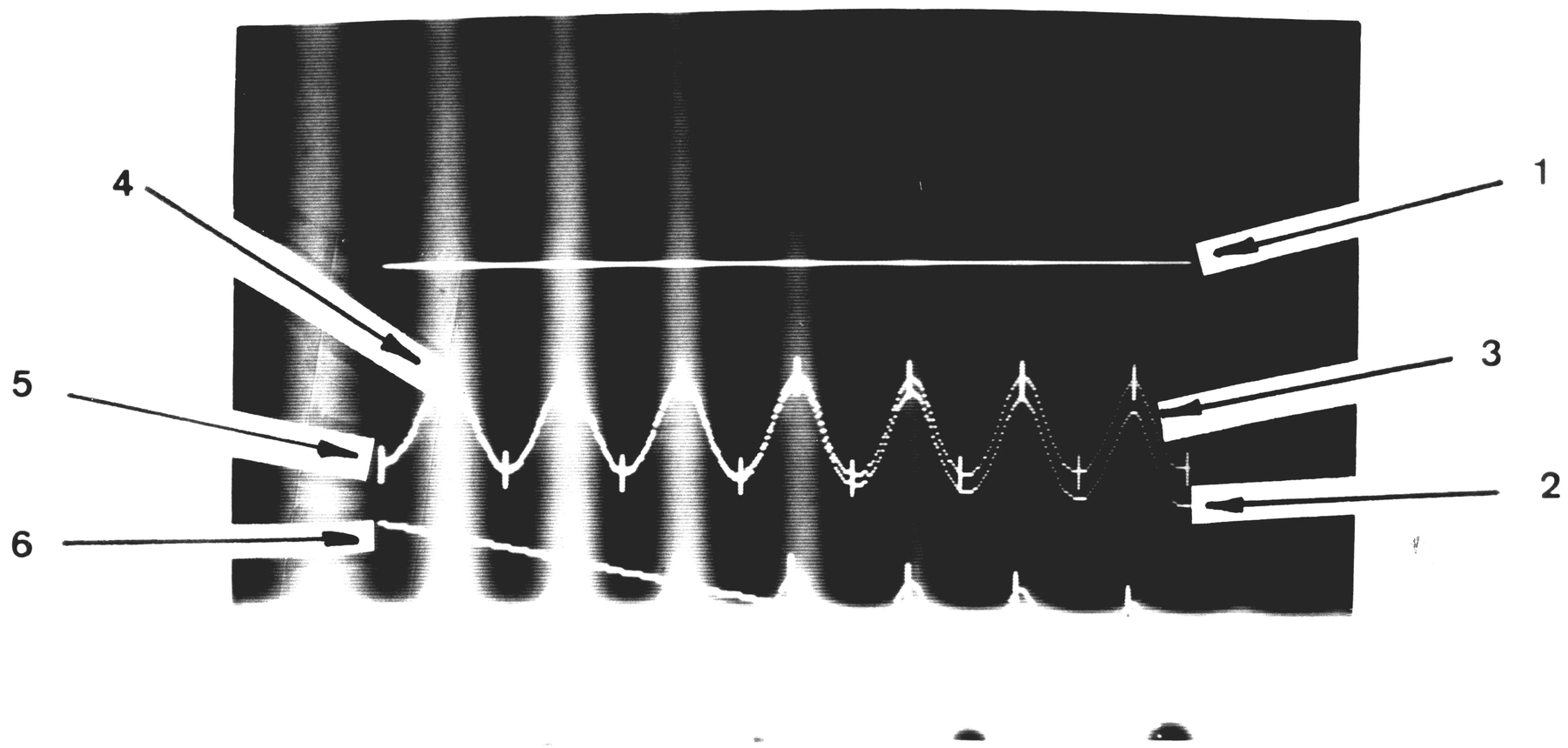

Density 50 lines/inch

Figure 7.1 Shadow Moire Image(wedge geometry)

1. Scan line
2. Original light intensity along the scan line
3. Light intensity after taking into account of non-uniform light field
4. Peak of bright fringe
5. Peak of dark fringe
6. Out-of-plane displacement

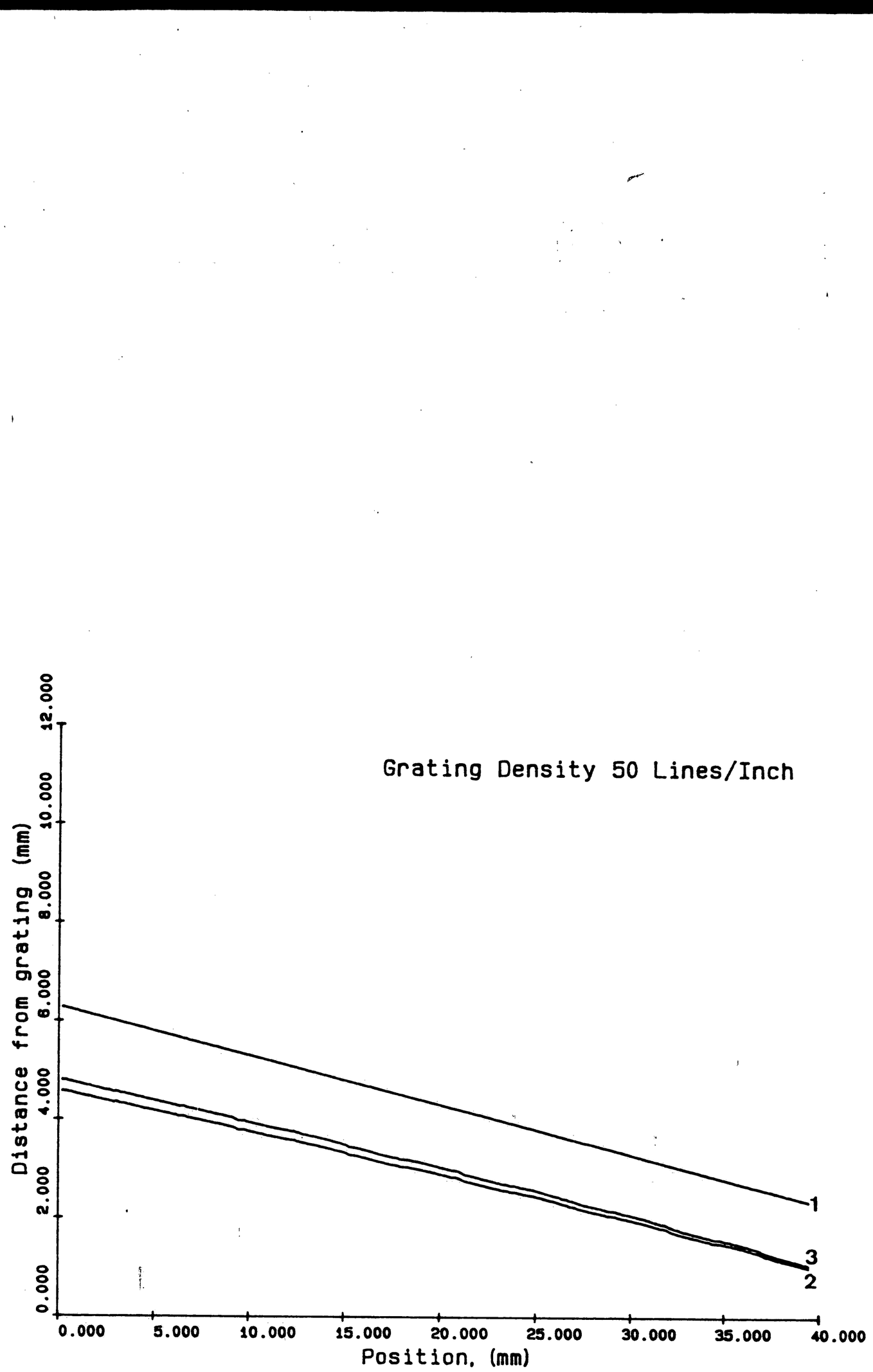

Fig. (7 2 Distance from the grating along the scan line
1 - Actual depth measured by dial gage
2 - Distance calculated from shadow moire pattern
3 - Distance calculated from shadow moire pattern
Taking into account correct angle of light incidence

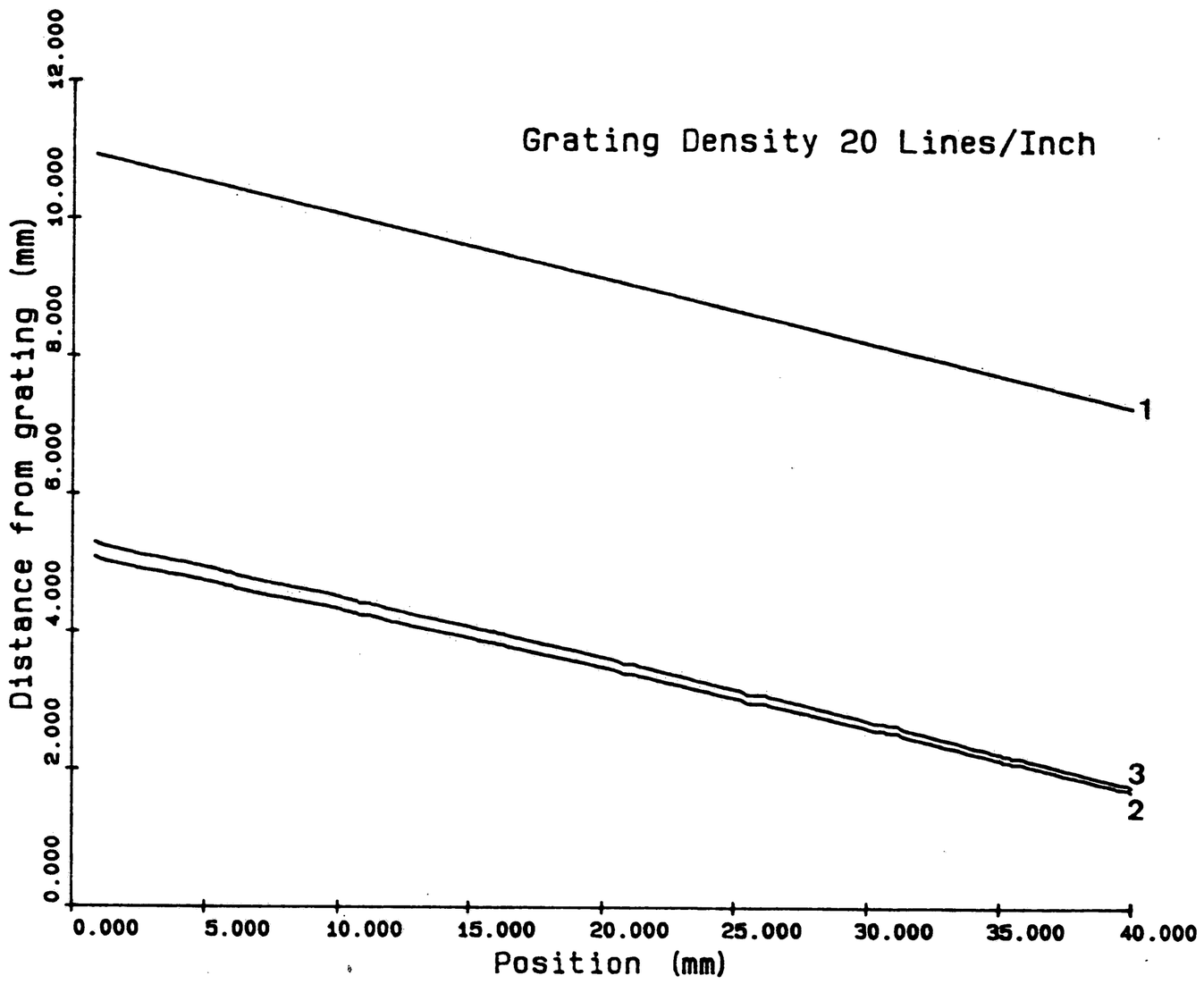

Fig. (7 3 Distance from the grating along the scan line
1 - Actual depth measured by dial gage
2 - Distance calculated from shadow moire pattern
3 - Distance calculated from shadow moire pattern
Taking into account correct angle light incidence

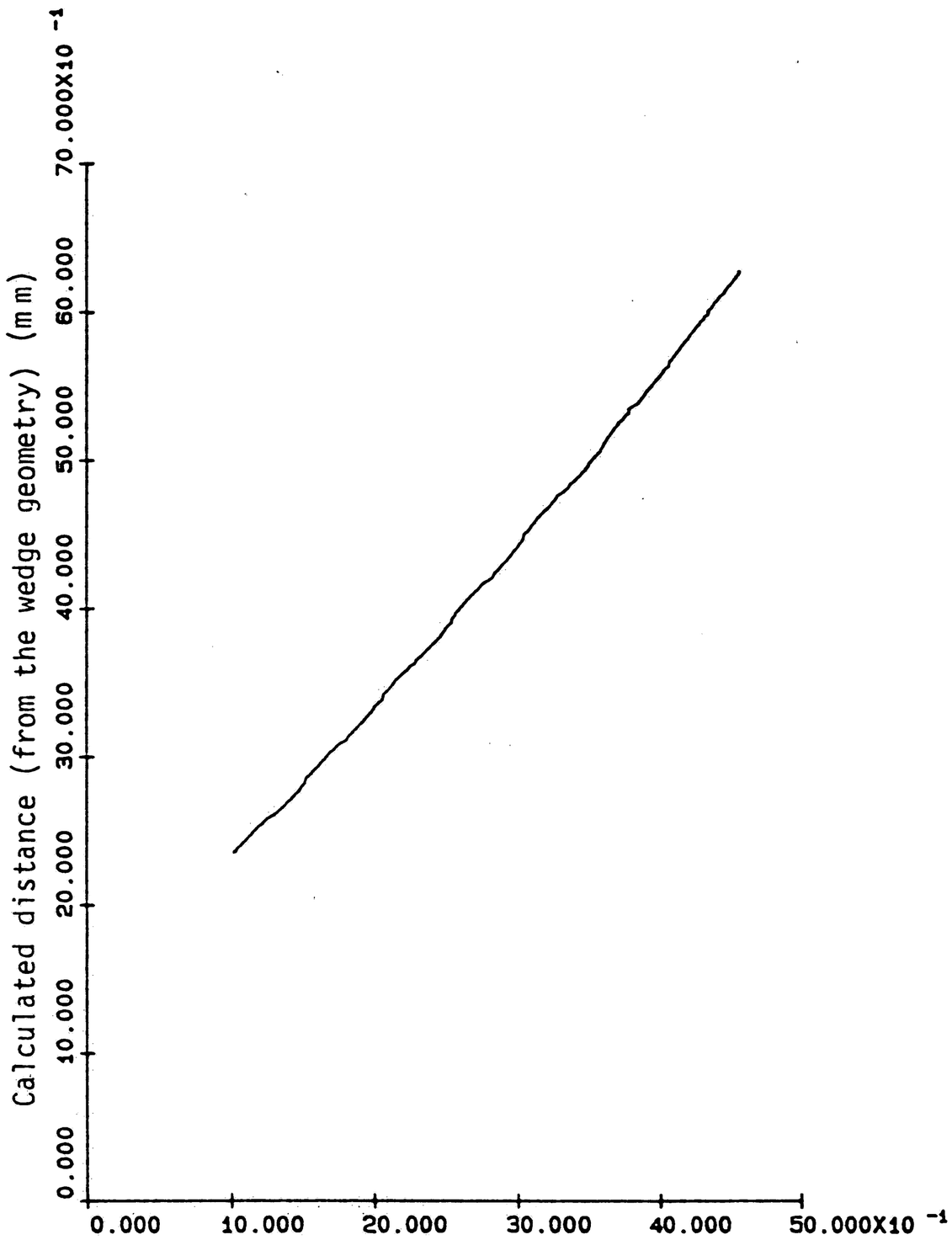

Fig. 74 Calibration of the experimental setup.(20 l./in.)

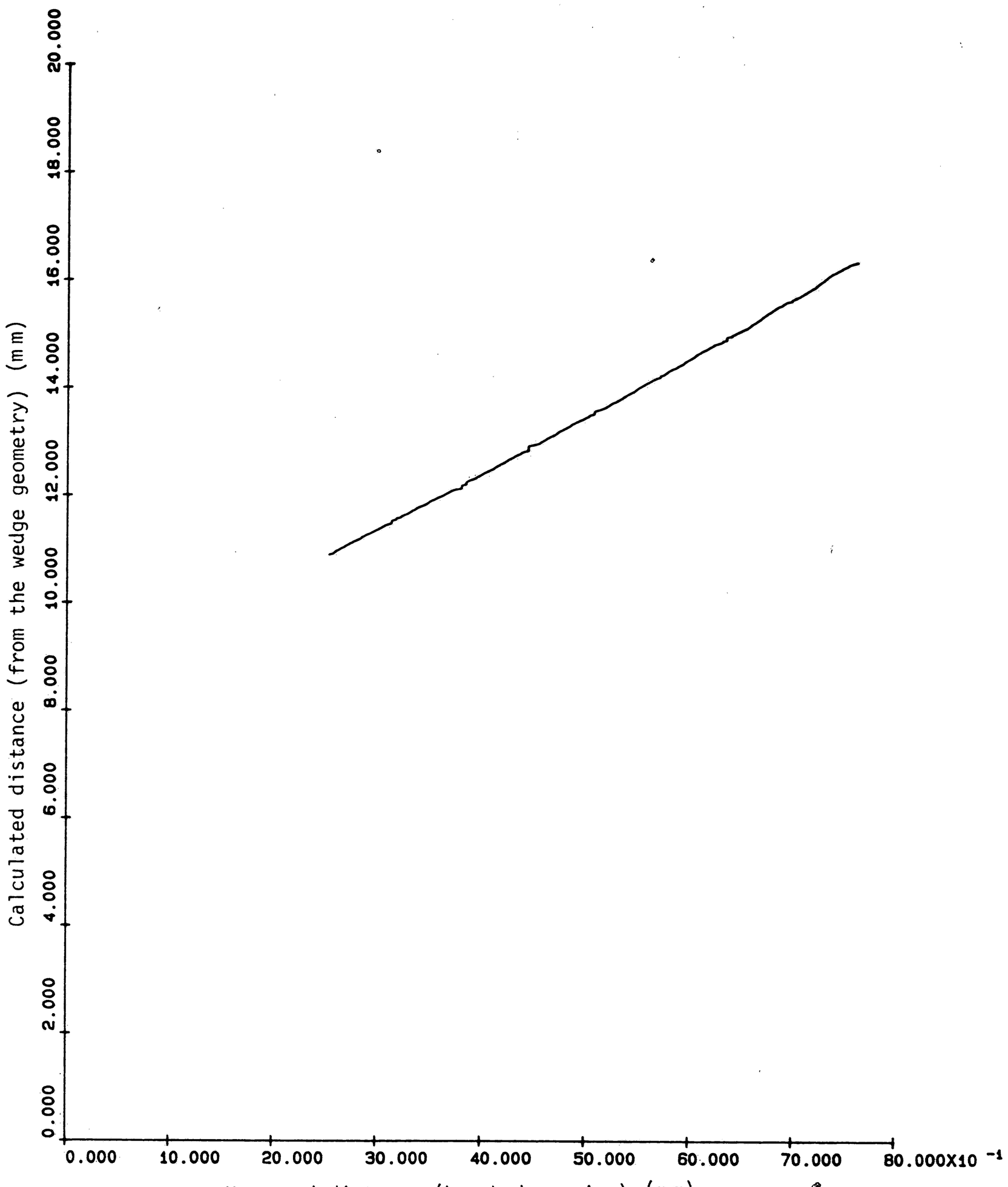

Fig. (**7 5** Calibration of the experimental setup. (50 l./in.)

8. CONCLUSIONS

The shadow moire technique is a simple and straight forward approach for measurement of the specimen topology. There is no need to cement any sensor to the specimen, there is no contact between the measuring device and the surface that is examined. The shadow moire technique is applicable to flat or curved surfaces, the apparatus can be used in the laboratory or in the field and it is relatively insensitive to temperature, humidity,and vibration.

The average relative error difference between the shadow moire data and the dial gage data, which was about 2.5 percent may be explained by experimental noise, difficulties in scanning the edge of the image, and a possible rotation of the flat face of the specimen with respect to the master grating during the acquisition of the shadow moire image.

The experimental noise is the result of the imperfections in the plexiglas containing the grating such as dimples or scratches which may degrade the image; imperfections in the video camera lenses and electronics; nonuniformity of illumination due to imperfections in the light source; airborne dust particles between the light source and the specimen or in front of the camera; and reflections from the edge of the grating.

The possibility of rotation of the specimen with respect to the grating is present because the specimen is positioned with only one point in contact with the surface of the master grating. This rotation is apparent in the image of specimen 2 produced with pitch of 0.508 mm. The maximum error is located at both edges of the scan line. The largest factor creating error is the rotation of the specimen which can be observed in the contour plots.

Evidently, the shadow moire method is an accurate method for measuring out-of-plane displacements. It may be advantageous to improve the experimental apparatus in the area of positioning the specimen and grating, improving the light source, camera.

The shadow moire may be useful for nondestructive quality control such as the detection of inward and outward dimples and other surface deformations and defects. It also can be used for surface topology control of the part during manufacturing.

9. References

1. Theocaris, P.S. "Moire Fringes in Strain Analysis," Pergamon Press New York, 1969.

2. A. S. Voloshin, C.P. Burger, R.E. Rowlands "Fractional Moire Strain Analysis Using Digital Image Analysis Techniques," Experiemtal Mechanics, 1986.

3. Takasaki, H. "Moire Topography," Applied Optic 12(2) 845-850, 1973.

4. Asundi, A. and Cheung, M.T. "Moire Interferometry for Out-of-Plane Displacement Measurement," Journal of Strain Analysis 21(1) 51-54, 1986.

5. Theocaris, P.C. " Isoparhic Pattern by the Moire Method," Experimental Mechanics 4(6) 153-159, 1964.

6. Dykes, B.C. "Analysis of Displacement in Large Plates by the Grid-Shadow Moire Technique', Experimental Stress Analysis and Its Influence on Design," Processings of the 4th International Conference on Experimental Stress Analysis 125-134, 1971.

7. Sciammarella, C. A. "Basic Optical Law in the Interpretation of Moire Pattern Applied to the Analysis of Strain-part 1," Experimental Mechanics 5(5), 154-160. 1965.

8. Chiang, Fu-pen " A Shadow-Moire Method with Two Discrete Sensitivities," Experimental Mechanics 15(10), 114-124, 1975.

9. A.J. Durelli "Moire Analysis of strain," Chapter 14

10. Sony service manual XCM-57.

11. DT_IRIS data translation manual UM-05633-A.

12. Collt, J. P. et al. " Le moire D'Ombre : Une Methode Experimental etses Possibilities," Bulletin Technique de la suisse Romande. 9, 179-189, April 1974.

13. Brown, A. L. "Contouring The Tire Sidewall with Moire Fringes," General Motors Research Publication GRM-1410, 1970.

14. Williams, J. G. "Effects of Impact Damage on the Compression Strength of Tough Resin/High Strain Fiber laminates," NASA TM 85756, 1984.

10. Vita

Andrew Liao came to The United States after completing an education at the St John's & St Mary's Institute of Technology in Taiwan. In 1987 he received a bachelor's degree in Mechanical Engineering from The University of Arizona. He chose to take the master degree program at Lehigh University. In 1990 he received the master degree of Mechanical Engineering from Lehigh University. Now he is employed as a mechanical engineer at a hydraulic corporation.